

2019-04-09


## Genome-Scale CRISPR Screens Identify Human Pluripotency-Specific Genes

Robert J. Ihry  
*Novartis Institutes for Biomedical Research*

*Et al.*

Let us know how access to this document benefits you.

Follow this and additional works at: <https://escholarship.umassmed.edu/oapubs>

 Part of the [Cell Biology Commons](#), [Cells Commons](#), [Computational Biology Commons](#), [Developmental Biology Commons](#), [Genetics Commons](#), [Genomics Commons](#), [Investigative Techniques Commons](#), [Molecular Genetics Commons](#), and the [Nucleic Acids, Nucleotides, and Nucleosides Commons](#)

---

### Repository Citation

Ihry RJ, Yang Z, Kaykas A. (2019). Genome-Scale CRISPR Screens Identify Human Pluripotency-Specific Genes. Open Access Articles. <https://doi.org/10.1016/j.celrep.2019.03.043>. Retrieved from <https://escholarship.umassmed.edu/oapubs/3821>

Creative Commons License



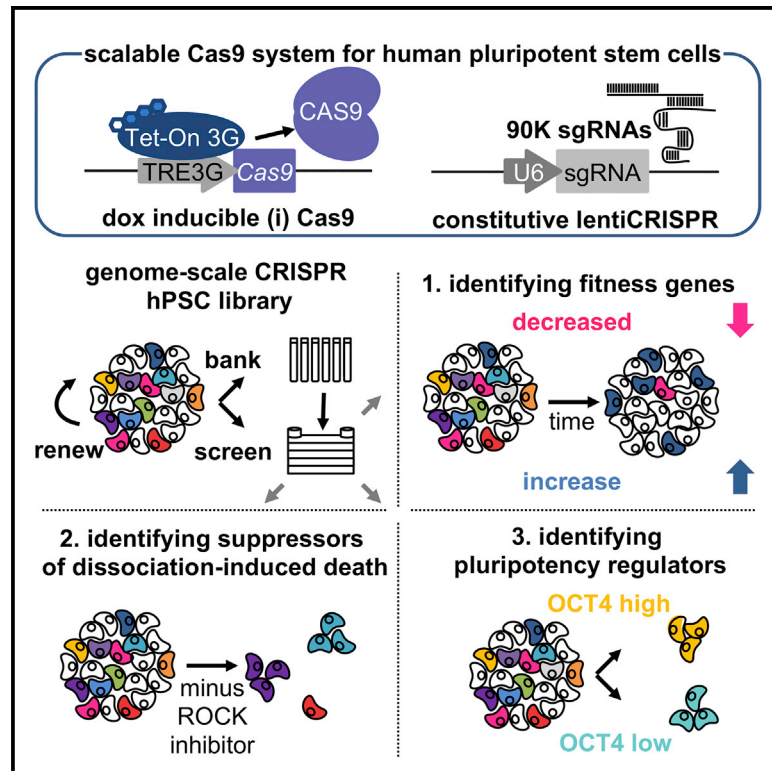
This work is licensed under a [Creative Commons Attribution 4.0 License](#).

This material is brought to you by eScholarship@UMMS. It has been accepted for inclusion in Open Access Articles by an authorized administrator of eScholarship@UMMS. For more information, please contact [Lisa.Palmer@umassmed.edu](mailto:Lisa.Palmer@umassmed.edu).

# Cell Reports

## Genome-Scale CRISPR Screens Identify Human Pluripotency-Specific Genes

### Graphical Abstract



### Authors

Robert J. Ihry, Max R. Salick, Daniel J. Ho, ..., Gregory R. Hoffman, Ricardo Dolmetsch, Ajamete Kaykas

### Correspondence

robert.ihry@novartis.com (R.J.I.), akaykas@gmail.com (A.K.)

### In Brief

Ihry et al. develop a CRISPR/Cas9 genetic screening platform for hPSCs that enables unbiased genome-scale genetic screening. The platform exhibits high performance and accurately detects the dropout of essential genes. Furthermore, proof-of-concept screens exploit hPSC-specific phenotypes to identify regulators of fitness, survival after single-cell dissociation, and pluripotency.

### Highlights

- A universal and scalable genetic platform in hPSCs for general use across all lineages
- Robust knockout efficiencies translate into high-performance screening at genome scale
- Stem cell-specific components of *TP53* and *OCT4* genetic networks in hPSCs are identified
- Validation of *PMAIP1* and *PAWR* function in sensitivity to DNA damage or dissociation



# Genome-Scale CRISPR Screens Identify Human Pluripotency-Specific Genes

Robert J. Ihry,<sup>1,\*</sup> Max R. Salick,<sup>1,7</sup> Daniel J. Ho,<sup>1</sup> Marie Sondey,<sup>1,3</sup> Sravya Kommineni,<sup>1,8</sup> Steven Paula,<sup>2</sup> Joe Raymond,<sup>1</sup> Beata Henry,<sup>1</sup> Elizabeth Frias,<sup>2</sup> Qiong Wang,<sup>2</sup> Kathleen A. Worringer,<sup>1</sup> Chaoyang Ye,<sup>1,4</sup> Carsten Russ,<sup>2</sup> John S. Reece-Hoyes,<sup>2</sup> Robert C. Altshuler,<sup>1</sup> Ranjit Randhawa,<sup>1,5</sup> Zinger Yang,<sup>2,6</sup> Gregory McAllister,<sup>2,9</sup> Gregory R. Hoffman,<sup>2,9</sup> Ricardo Dolmetsch,<sup>1</sup> and Ajamete Kaykas<sup>1,7,10,\*</sup>

<sup>1</sup>Department of Neuroscience, Novartis Institutes for Biomedical Research, Cambridge, MA 02139, USA

<sup>2</sup>Department of Chemical Biology and Therapeutics, Novartis Institutes for Biomedical Research, Cambridge, MA 02139, USA

<sup>3</sup>Abbvie, Cambridge, MA 02139, USA

<sup>4</sup>Blueprint Medicines, Cambridge, MA 02139, USA

<sup>5</sup>Axcella Health, Cambridge, MA 02139, USA

<sup>6</sup>University of Massachusetts Medical School, Worcester, MA 01655, USA

<sup>7</sup>Insitro, South San Francisco, CA 94080, USA

<sup>8</sup>Casma Therapeutics, Cambridge, MA 02139, USA

<sup>9</sup>Sana Biotechnology, Cambridge, MA 02139, USA

<sup>10</sup>Lead Contact

\*Correspondence: [robert.ihry@novartis.com](mailto:robert.ihry@novartis.com) (R.J.I.), [akaykas@gmail.com](mailto:akaykas@gmail.com) (A.K.)

<https://doi.org/10.1016/j.celrep.2019.03.043>

## SUMMARY

Human pluripotent stem cells (hPSCs) generate a variety of disease-relevant cells that can be used to improve the translation of preclinical research. Despite the potential of hPSCs, their use for genetic screening has been limited by technical challenges. We developed a scalable and renewable Cas9 and sgRNA-hPSC library in which loss-of-function mutations can be induced at will. Our inducible mutant hPSC library can be used for multiple genome-wide CRISPR screens in a variety of hPSC-induced cell types. As proof of concept, we performed three screens for regulators of properties fundamental to hPSCs: their ability to self-renew and/or survive (fitness), their inability to survive as single-cell clones, and their capacity to differentiate. We identified the majority of known genes and pathways involved in these processes, as well as a plethora of genes with unidentified roles. This resource will increase the understanding of human development and genetics. This approach will be a powerful tool to identify disease-modifying genes and pathways.

## INTRODUCTION

Human pluripotent stem cells (hPSCs) can be used to generate a wide variety of disease-relevant cell types and have the potential to improve the translation of preclinical research by enhancing disease models. Despite the huge potential, genetic screening using hPSCs has been limited by their expensive and tedious cell culture requirements (Chen et al., 2011) and reduced genetic manipulation efficiencies (Ihry et al., 2018). Only a few short hairpin RNA (shRNA) screens have been conducted in hPSCs

(Chia et al., 2010; Zhang et al., 2013), but shRNAs have a high level of off targets and do not cause a complete loss of function, which is difficult to interpret (DasGupta et al., 2005; Echeverri et al., 2006; Kampmann et al., 2015; McDonald et al., 2017). Currently, the CRISPR/Cas9 system is the genetic screening tool of choice because it can efficiently cause loss-of-function alleles (Jinek et al., 2012; Cong et al., 2013; Mali et al., 2013). Hundreds of genome-scale pooled CRISPR screens have been performed in immortalized human cell lines (Hart et al., 2015; Wang et al., 2015; Meyers et al., 2017). However, in hPSCs the CRISPR/Cas9 system has been used primarily for small-scale genome engineering (Merkle et al., 2015). In genetically intact hPSCs, the only genome-scale CRISPR screen to date used methods developed for cancer cells, suffered from technical issues, had poor performance, and identified few developmentally relevant genes (Hart et al., 2014; Shalem et al., 2014). We addressed these technical issues by systematically tailoring the CRISPR/Cas9 system for hPSCs (Ihry et al., 2018). We developed a doxycycline (dox)-inducible Cas9 (iCas9) hPSC line and stably infected it with a genome-scale single guide RNA (sgRNA) library. We banked and expanded the CRISPR-infected hPSC library in the absence of editing (–dox), which enabled us to generate a renewable stem cell pool with stable but inactive sgRNAs. This allowed us to conduct multiple independent screens with the same cell library.

In the first screen, we identified genes that suppress or enhance hPSC fitness over long-term culture. Although previous screens have generated gold-standard gene lists of core-essential genes that reduce cell survival when mutated, little is known about the mutations that enhance survival and proliferation. Unlike core-essential genes, these enhancing mutations appear to be cell type specific, and no consistent lists exist for this type of gene (Hart et al., 2014). In hPSCs, karyotypic analysis has detected recurrent copy number variations (CNVs) that confer a growth advantage (Amps et al., 2011; Laurent et al., 2011); however, these studies lack gene level resolution. Recently, next-generation



sequencing of hundreds of hPSCs identified the recurrence of dominant-negative *TP53* mutations that can expand within a population of hPSCs (Merkle et al., 2017). We mined our data for gene knockouts that enriched in culture and identified many genes, including components of the *TP53* pathway and other known tumor suppressors. We validated the strongest hit, *PMAIP1/NOXA*, which appears to be a stem cell-specific gene conferring sensitivity to DNA damage downstream of *TP53*.

In the second screen, we identified genes required for single-cell cloning. hPSCs have a poor survival rate after dissociation to single cells, which is detrimental for genome engineering. Multiple groups have extensively characterized death induced by single-cell cloning and have demonstrated the process is similar to but distinct from anoikis and is triggered by a ROCK/myosin/actin pathway (Chen et al., 2010; Ohgushi et al., 2010). To prevent death, hPSCs are passaged as clumps or treated with ROCK inhibitors (Watanabe et al., 2007). By subjecting our hPSC mutant library to single-cell dissociation without ROCK inhibitors, we selected for mutations that survive single-cell cloning. sgRNAs for the ROCK and myosin pathways were enriched in the surviving clones. The most enriched gene was the proapoptotic regulator *PAWR* (Burikhanov et al., 2009). Validation studies confirmed a role for *PAWR* as a component of the actin-cytoskeleton that induces membrane blebbing and cell death caused by single-cell cloning. The additional genes identified here will further our understanding about the sensitivity of hPSCs to single-cell cloning.

In the final screen, we used a fluorescence-activated cell sorting (FACS)-based OCT4 assay to identify regulators of pluripotency and differentiation. Pluripotency is a defining feature of hPSCs, and it allows them to differentiate into all three germ layers. *OCT4/POU5F1*, *NANOG*, and *SOX2* are critical transcription factors that maintain pluripotency *in vivo* and *in vitro* (Nichols et al., 1998; Chambers et al., 2007; Masui et al., 2007). *OCT4* and *SOX2* overexpression is commonly used to reprogram somatic cells toward the pluripotent state (Takahashi and Yamanaka, 2006; Takahashi et al., 2007; Yu et al., 2007). By isolating mutant cells with high or low OCT4 protein expression, we identified many genes involved in maintaining the pluripotent state, along with genes involved with induction of differentiation.

By using an iCas9 hPSC line stably infected with a genome-scale lentiCRISPR library, we were able to bank a CRISPR-hPSC library that was renewable and enabled a large number of independent screens with the same starting library. This allows direct comparison between screens and reduces screen to screen variability. We rigorously tested the system and identified genes important for fitness, single-cell cloning, and pluripotency of hPSCs. Herein we provide a resource with detailed methods and all available data including many genes that are involved in hPSC biology. This resource will serve as a parts list of genes that are functionally important for the human stem cell state. These lists of genes provide unique insights into the genetic regulation of human development that could only be identified in normal diploid cells that are not transformed or cancerous. Furthermore, the gene sets and methods will increase our systematic knowledge of hPSC biology and will enable additional large-scale CRISPR screens in stem cells and their somatic derivatives.

## RESULTS

### The iCas9 System Is a Self-Renewing Resource Enabling Successive Genome-wide Genetic Screens in hPSCs

We set out to develop a high-throughput CRISPR/Cas9 platform for hPSCs that would enable successive rounds of screening from a stable library of lentiCRISPR-infected hPSCs (Figures 1A and S1). Generating a genome-scale lentiCRISPR hPSC library would enable both the rigorous testing of CRISPR screen performance and the identification of cell type-specific regulators of the pluripotent state. In our previous work, we developed an all-in-one iCas9 transgene that was inactive in the absence of dox (Ihry et al., 2018). The tight control over Cas9 expression allowed us to transduce cells with lentiviruses expressing sgRNAs (lentiCRISPRs) in the absence of dox without causing on-target indels. We tested if it was possible to bank a genome-scale lentiCRISPR-infected cell library (~5 sgRNAs per gene, 91,725 total sgRNAs) prior to Cas9 mutagenesis (–dox). After one freeze-thaw cycle, next-generation sequencing (NGS) analysis revealed no bottlenecks of the library demonstrating the feasibility of banking a large lentiCRISPR hPSC library for repeated screens (Figure 1B).

### Evaluating the Performance of CRISPR Screening in iCas9 hPSCs

Next, we performed a fitness screen to evaluate the global performance of the system (Figure 1C). We benchmarked the performance of the screen by using annotated lists of core-essential genes. Core-essential genes are required for the survival of all cells; the corresponding CRISPR knockout causes the sgRNAs to be depleted (Hart et al., 2014, 2015). Genome-scale CRISPR screening in hPSCs has been challenging (Hart et al., 2014; Shalem et al., 2014). hPSCs have a strong DNA damage response (DDR), and Cas9-induced double-strand breaks (DSBs) cause a significant cell loss (Ihry et al., 2018). Failure to account for Cas9-induced cell loss is problematic for pooled screening, because it is critical to maintain representation of each sgRNA-barcoded cell. Our previous work demonstrated a range of Cas9-induced cell loss between 3- and 10-fold across many sgRNAs (Ihry et al., 2018). To reduce the bottlenecks of the sgRNA library caused by Cas9-induced toxicity, we started the screen in hPSCs at an average of 1,200 cells per sgRNA (a total of 110 million infected cells). By doing this we maintained about 4-fold more cells than a typical cancer screen (Hart et al., 2015). During the fitness screen, DNA was sampled before and after dox exposure at days 0, 8, 14, and 18 (Figure S1). To provide a qualitative measurement of screen performance, we plotted the p values calculated by the redundant small interfering RNA (siRNA) activity (RSA) test against Q1 based Z scores for a set of core-essential and non-essential genes (König et al., 2007; Hart et al., 2014). Before dox treatment the non-essential and core-essential genes are randomly distributed within a tight cluster (Figure 1D). After 18 days of Cas9 treatment, the distribution spreads, and the essential genes significantly drop out while the non-essential genes remain constant (Figure 1D; Tables S1 and S2).

To quantify performance, we used the Bayesian analysis of gene essentiality (BAGEL) algorithm, which calculates a Bayes

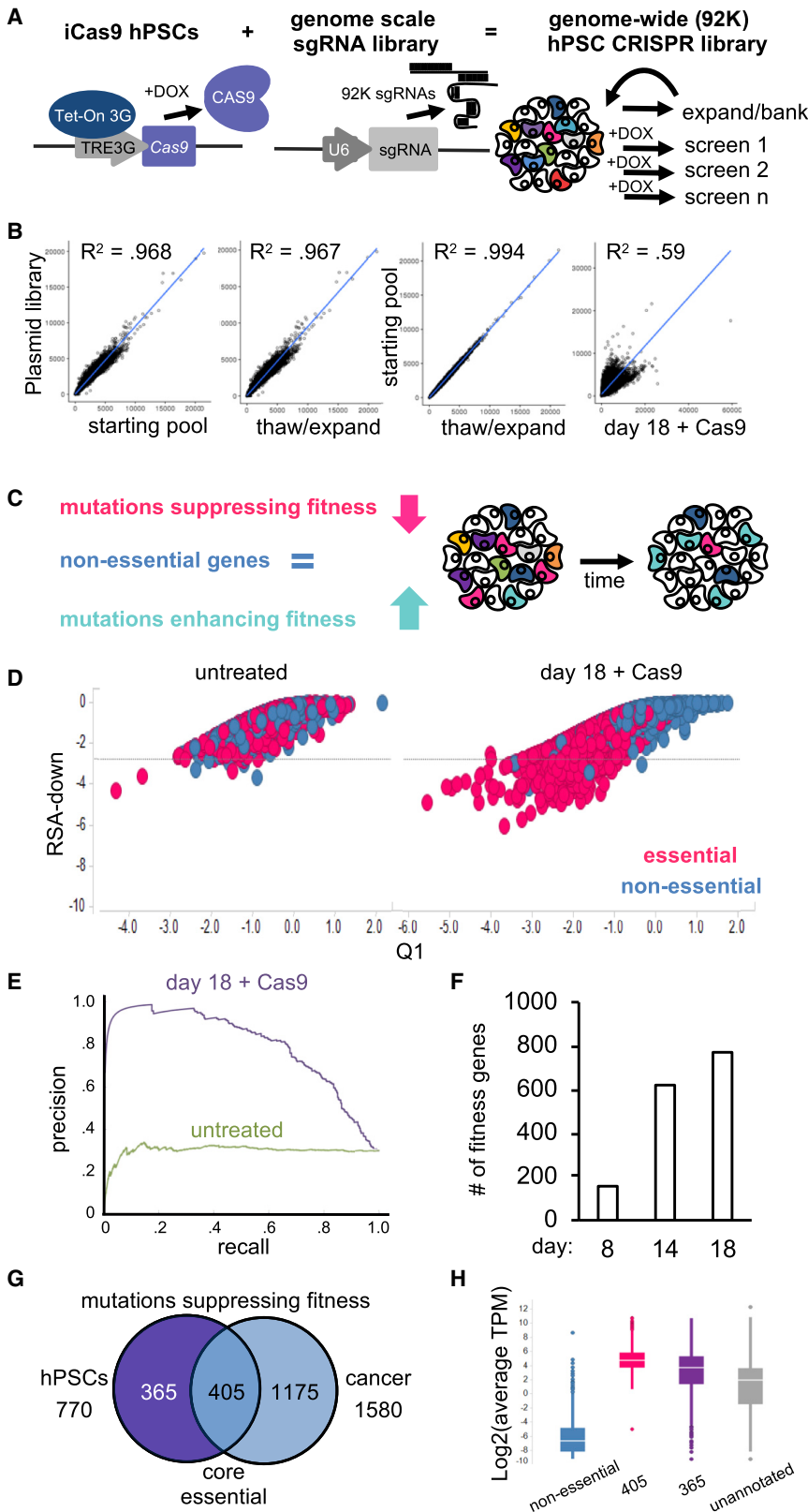


**Figure 1. A Self-Renewing Dox-Inducible CAS9 Genome-wide sgRNA Cell Library Enables Multiple High-Performance CRISPR Screens in Human Pluripotent Stem Cells**

(A) Diagram depicting the iCas9 platform for genome-scale CRISPR screening in hPSCs. The iCas9 platform consists of a dox-inducible Cas9 transgene knocked in the AAVS1 locus of H1-hESCs and lentiviral delivery of constitutively expressed sgRNAs. iCas9 hPSCs were transduced (.5 MOI) at scale. After 1 week of expansion and selection for lentiCRISPRs, iCas9 hPSCs were either banked or subjected to Cas9 mutagenesis for screening.

(B) Correlation of normalized sgRNA counts reveals that freeze and thaw expanded samples (-dox) have high correlation with the plasmid library and the starting pool of infected iCas9 hPSCs at day 0 of the screen. Day 18 samples have been exposed to dox (+Cas9).  $R^2$  values were calculated on the basis of the normalized count values.

(C) Diagram depicting three categories of genes that enrich (enhance), deplete (suppress), or remain constant during a fitness screen.

(D) Scatterplot depicting gene level results for core-essential (pink) and non-essential (blue) genes. Without Cas9 treatment (-dox), cells expressing sgRNAs targeting core-essential and non-essential genes are interspersed and have an  $RSA > -2.75$  (marked by dashed line). After 18 days of exposure to Cas9 (+dox), sgRNAs targeting essential genes drop out to less than  $RSA < -2.75$ . The y axis is RSA value, and the x axis marks the Z score (Q1). Non-essential and core-essential gene list from Hart et al. (2014).

(E) Precision recall (PR) analysis of genome-scale CRISPR screening data in H1-hESCs. Cas9-expressing cells (purple) exhibit a PR curve that gradually slopes off, whereas cells without Cas9 (green) exhibit a PR curve that immediately decreases.

(F) Fitness gene calculation on the basis of 5% false discovery rate (FDR) on the y axis. Each condition labeled on the x axis.

(G) Venn diagram comparing 770 depleted genes in hPSCs with 1,580 core-essential genes identified by screening cancer cell lines (Hart et al., 2015). 405 of the hPSCs depleted genes overlap, while the remaining 365 are specifically depleted in pluripotent stem cells.

(H) Genes that dropout in CRISPR screen are abundantly expressed. The y axis depicts the log<sub>2</sub> transformation of average TPM values from 20 independent RNA-seq experiments in H1-hESC. For each box blot, the median is depicted by white line flanked by a rectangle spanning Q1-Q3. The x axis depicts gene categories. In blue are non-essential genes from Hart et al. (2014), in pink are 405 core-essential genes, in purple are 365 stem cell-specific essential genes, and in gray are the remaining unannotated genes.

See also Figure S1.



factor for each gene by determining the probability that the observed fold change for a given gene matches that of known essential genes (Hart and Moffat, 2016). This generates a ranked list of Bayes factors for each gene, which can then be used to quantify screen performance by precision versus recall analysis. In a high-performance screen, essential genes have high Bayes factor scores, and the precision versus recall curve gradually drops off as analysis of the ranked list is completed. In contrast, a poor-performing screen has a precision versus recall curve that rapidly drops off, indicating many false positives (non-essential genes) with high Bayes factor scores. The sample without dox exposure (untreated) has a randomly ranked Bayes factor list with non-essential and essential genes interspersed and exhibits a poor precision versus recall curve (Figure 1E). In the day 18 Cas9 (+dox) treated samples, essential genes and non-essential genes segregate from each other and generates a high-performing precision versus recall curve that gradually drops off (Figure 1E; Table S3).

After 18 days of Cas9 exposure, we identified 770 fitness genes at a 5% false discovery rate on the basis of the precision calculation (Figure 1F; Table S4). Comparing the set of 770 hPSC fitness genes with 1,580 core-essential genes from cancer lines revealed an overlap of 405 genes (Figure 1G) (Hart et al., 2015). The remaining 365 specifically dropped out in hPSCs. Both the core and hPSC-specific essential genes are abundantly expressed in hPSCs, further supporting that they are required to maintain hPSCs in culture (Figure 1H). Our fitness screen in hPSCs correctly identifies the dropout of core-essential genes with accuracy that is on par with CRISPR screens conducted in cancer cell lines. This demonstrates that cancer cells and stem cells share a common set of core-essential genes that can be used to benchmark performance. By accounting for cell loss caused by Cas9 activity, we limited the effects of Cas9-induced toxicity that have thwarted previous attempts at genome-scale screening in hPSCs (Hart et al., 2014; Shalem et al., 2014). This demonstrates that it is possible to conduct an effective genome-scale CRISPR screen in hPSCs using the methods described here.

### **TP53 Pathway Mutations Specifically Enrich during CRISPR Fitness Screen in hPSCs**

Curated lists of genes that enhance fitness during a CRISPR screen do not exist, making it difficult to benchmark the enrichment results (Hart et al., 2015). By comparing the top ~1,000 depleted (RSA-down < -2.25; Table S2) and enriched (RSA-up < -2.25; Table S5) genes, we observed that 31.8% (301 of 946) of the enriched genes were located on the X and Y chromosomes (H1-human embryonic stem cells [hESCs] XY; Figure S3). In contrast, the depleted genes were evenly distributed across all chromosomes. It became apparent that allosome-targeting sgRNAs were behaving similarly to non-targeting controls, which enrich during a CRISPR screen in hPSCs (Ihry et al., 2018). We observed that sgRNAs causing a single DSB on the X chromosome are less toxic relative to sgRNAs inducing two DSBs at the *MAPT* locus despite being able to efficiently induce indels (Figure S2). sgRNAs targeting genomic amplifications in cancer cell lines exhibit a strong depletion irrespective of the gene targets (Aguirre et al., 2016; Munoz et al.,

2016; Meyers et al., 2017). Unlike cancer cell lines, H1-hESCs with a normal diploid karyotype are very sensitive to DNA damage, making the difference between one and two DSBs significant. After recognizing that the enrichment of sgRNAs on the X and Y chromosomes was related to DSB sensitivity and copy number differences in male H1-hESCs, we focused on autosomal genes. In the remaining list of 645 autosomal genes that were enriched (RSA-up -2.25), we identified 41 tumor suppressor genes (Zhao et al., 2016).

The second most enriched gene was *TP53*, which confirms the selective pressure imposed by Cas9-induced DSBs in hPSCs during a CRISPR screen (Figure 2A). Consistent with this *TP53* mutants are able to suppress cell loss induced by Cas9 activity (Ihry et al., 2018). Throughout the 18-day screen, the representation of sgRNAs targeting *TP53* (chromosome [Chr.] 17), the checkpoint kinase *CHEK2* (Chr. 22), and the pro-apoptotic regulator *PMAIP1* (Chr. 18) increased in a time-dependent manner (Figure 2B). Database mining for associations with *TP53* among the enriched genes identified 20 genes with direct connections to *TP53* (Figure 2C; Table S6), 19 of which are expressed in H1-hESC and are on autosomal chromosomes. Although *EDA2R* is on the X chromosome, it was included because its mRNA increases in response to DNA damage in hPSCs (Ihry et al., 2018). We hypothesized that these genes could include additional regulators responsible for the extreme sensitivity to DNA damage in hPSCs.

*PMAIP1* was the most enriched gene in the screen. *PMAIP1* has been implicated in *TP53*-dependent cell death and functions by sensitizing cells to apoptosis by antagonizing the anti-apoptotic protein MCL1 at the mitochondria (Kim et al., 2006; Ploner et al., 2008; Perciavalle et al., 2012). *PMAIP1* is highly expressed in hPSCs, and its expression marks the pluripotent state (Mallon et al., 2013). We confirmed this by examining *PMAIP1* expression in two induced pluripotent stem cell (iPSC) and two hESC lines. Analysis of RNA sequencing (RNA-seq) experiments confirmed that *PMAIP1* was highly expressed during the pluripotent state and drops during neuronal differentiation using the *NGN2* transgene (Figure 3A). Additionally, Genotype-Tissue Expression (GTEx) data revealed that *PMAIP1* has a highly restricted expression pattern and is not expressed in most tissues (GTEx Analysis Release V7). Although it has been demonstrated that *PMAIP1* expression is maintained by *OCT4* in testicular germ cell tumors (Gutekunst et al., 2013), no functional connection has been made in hPSCs. We tested if *PMAIP1* expression was maintained by the pluripotency network by differentiating cells or knocking out *OCT4*. Under these conditions qPCR detected a significant decrease in *PMAIP1* mRNA (Figure 3B). In thymocytes, *PMAIP1* mRNA is induced by TP53 (Khandanpour et al., 2013). We knocked out *TP53* in hPSCs but did not detect a reduction in *PMAIP1* mRNA (Figure 3B). hPSCs constitutively express high levels of *PMAIP1*, and DNA damage does not increase *PMAIP1* expression, further supporting *PMAIP1* mRNA as pluripotency dependent and TP53 independent (Ihry et al., 2018).

Prior work demonstrated that cancer cell lines have a reduced DDR relative to hPSCs (Ihry et al., 2018). Consistent with this, we did not observe an enrichment of *PMAIP1* sgRNAs in 14 independent CRISPR screens conducted in cancer cell lines despite

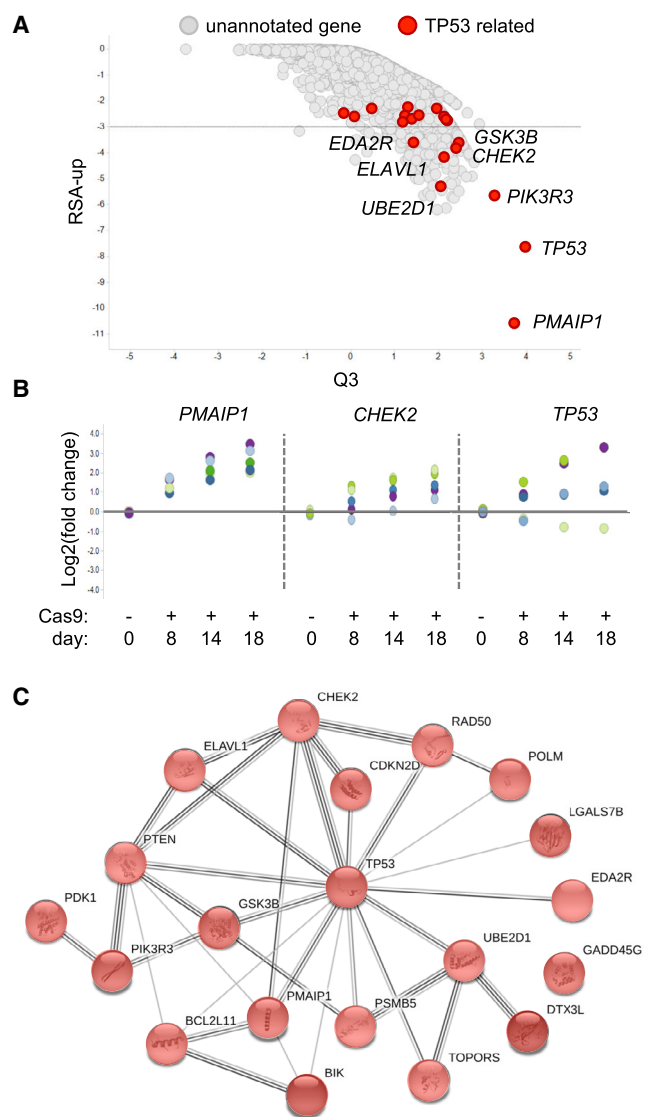


**Figure 2. TP53 Pathway Mutations Enrich during CRISPR Screen in hPSCs**

(A) Scatterplot depicting gene-level results for the genome-scale screen. After 18 days of exposure to Cas9 (+dox), sgRNAs targeting TP53-related genes enrich during the screen; *PMAIP1* (*NOXA*) (RSA  $-10.6$ , Q3 3.7), *TP53* (RSA  $-7.64$ , Q3 4), and *CHEK2* (RSA  $-3.6$ , Q3 2.4). A total of 302 genes have RSA scores  $< -3$  (marked by dashed line). TP53-related genes with RSA scores  $< -2.25$  are marked in red. The y axis is a p value generated from RSA-up analysis. The x axis marks the Z score (Q3).

(B) Plot showing the time-dependent increase in five independent sgRNAs targeting *PMAIP1*, *CHEK2*, and *TP53* during CRISPR screen. NGS quantifies representation of lentiCRISPR-infected cells. Samples were normalized to the day 0 population. The y axis represents log<sub>2</sub>(fold change). Day 0 data shown are from freeze and thaw samples. The x axis plots each condition over time. Cas9+ samples were treated with dox to induce Cas9 expression.

(C) Shown are gene knockouts (20) that enrich during CRISPR screen that are connected to *TP53* and play roles in either DNA damage response and apoptosis. 946 enriched genes in RSA-up  $< -2.25$  identified by STRINGdb analysis.

See also Figures S1 and S2.

using libraries containing the same *PMAIP1*-targeting sgRNAs (Figure 3C). This suggested that *PMAIP1* is responsible for making hPSCs sensitive to DNA damage. To test the functional consequences of *PMAIP1* mutations, we knocked out *PMAIP1* in the iCas9 cell line using transient exposure to synthetic crRNAs (Figure S3). We tested if *PMAIP1* mutants were resistant to DSB-induced death by using lentiCRISPRs to deliver a sgRNA targeting *MAPT*, a neuronal gene not expressed in hPSCs. In the absence of Cas9 (–dox), both control and *PMAIP1* mutant iCas9 cells grow at a similar rate while expressing an sgRNA. In the presence of Cas9 (+dox) and a sgRNA, control cells die, while *PMAIP1* mutants are able to survive despite efficient DSB induction (Figures 3D, S3, and S4E). qPCR analysis of the TP53-target genes *P21* and *FAS* detected an elevated expression in *PMAIP1* mutants compared with controls (Figure 3E). Despite having an active TP53, *PMAIP1* mutants survive. This indicates *PMAIP1* is downstream of TP53 activation and is consistent with its known role as a sensitizer to apoptosis (Ploner et al., 2008). In hPSCs, cell death is the predominant response to DNA damage. Unlike *PMAIP1* mutants, *P21* mutants (>80% indels) are unable to suppress DSB-induced toxicity (Figure S4E), and *P21* sgRNAs did not enrich in H1-hESCs. In contrast, in a genome-scale screen in retinal pigment epithelial cells, where Cas9 activity causes TP53-dependent cell-cycle arrest rather than apoptosis, sgRNAs targeting TP53 and *P21/CDKN1A* were enriched, while *PMAIP1* sgRNAs were not (Table S5) (Haapaniemi et al., 2017).

Overall, these results indicate that *PMAIP1* plays a role in the sensitivity of hPSCs to DNA damage and highlight the ability of genome-scale CRISPR screens to identify cell type-specific genes important for the fitness of pluripotent stem cells.

### Genetic Screen for Suppressors of Dissociation-Induced Death

We next tested our ability to identify phenotypic regulators of human developmental processes. Human PSCs, unlike mouse PSCs, are very sensitive to dissociation and die in the absence of ROCK inhibitors (Ohgushi et al., 2010). During dissociation of hPSCs, Rho and ROCK become activated. This leads to the phosphorylation of myosin, which causes membrane blebbing and cell death. To promote survival, inhibitors that target ROCK (Y-27632 or thiazovivin) or myosin (blebbistatin) are used routinely during hPSC passaging (Watanabe et al., 2007; Chen et al., 2010). Very few cells survive dissociation in the absence of ROCK inhibitors. Importantly, this phenotype is developmentally rooted. hPSCs are epiblast-like, and cells that fail to incorporate into the polarized epithelium of the epiblast undergo cell death in the embryo (Ohgushi et al., 2010). To gain a deeper understanding of the genes involved, we screened for suppressors of dissociation-induced death.

To ensure complete Cas9 mutagenesis, we waited till the day 14 passage of the fitness screen to plate an additional replicate of the genome-scale mutant cell library in the absence of thiazovivin (Figures 4A and S1). The majority of the mutant cells died during this process, and the surviving cells were maintained for 2 weeks until large colonies were visible, at which point DNA was isolated and sgRNAs sequences were recovered by NGS. We identified 76 genes with two or more independent sgRNAs present in cells that survived dissociation without thiazovivin

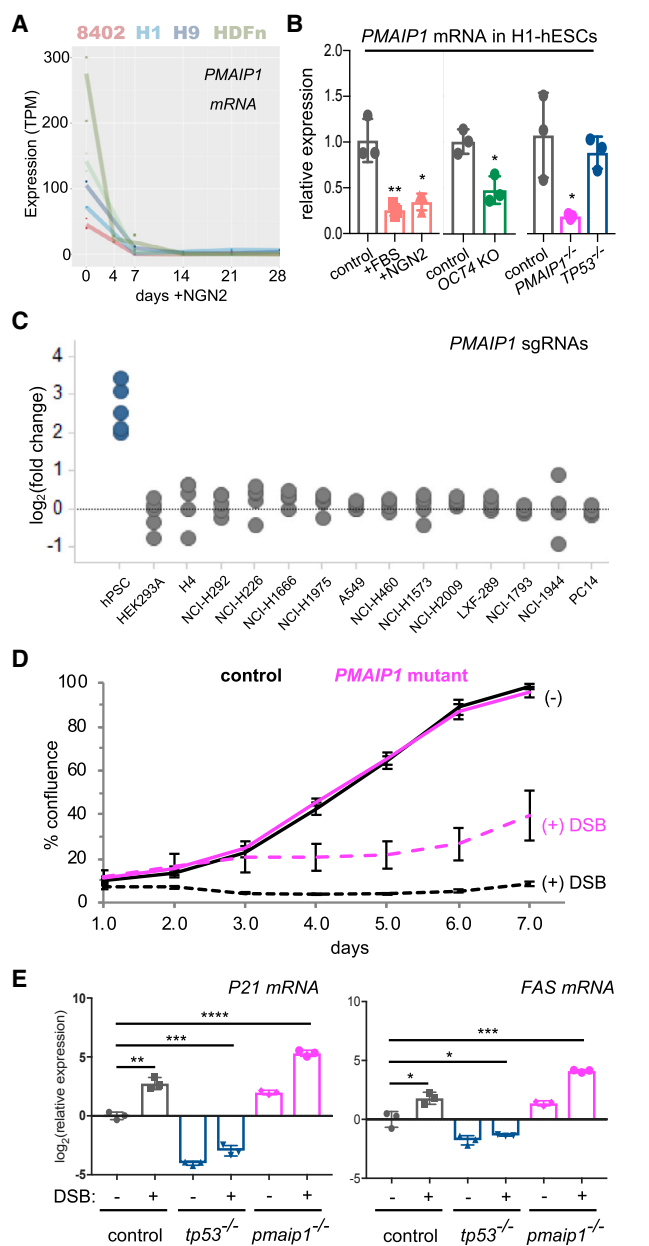


**Figure 3. *PMAIP1* Confers Sensitivity to DNA Damage in hPSCs**  
 (A) *PMAIP1* is highly expressed in hESCs and iPSCs. The y axis represents expression in transcripts per kilobase million (TPM). H1-hESCs (n = 1), H9-hESCs (n = 3), 8402-iPSCs (n = 3), and HDFn-iPSCs (n = 4). The x axis represents days after induction of a doxycycline-inducible NGN2 expression cassette. Day 0 = hPSCs.  
 (B) qPCR confirms that *PMAIP1* mRNA is dependent on the pluripotent state. The y axis is relative expression, and each bar represents mean relative expression. The x axis is each condition. Control, hPSCs in E8 media; +FBS, 3 days' exposure to 10% fetal bovine serum (FBS) and DMEM; +NGN2, 3 days' exposure to NGN2; *OCT4* KO, mutant pool after 6 days' exposure to iCas9 and sgRNA targeting *OCT4*; *PMAIP1*<sup>-/-</sup>, complete knockout cell line; *TP53*<sup>-/-</sup>, complete knockout cell line. n = 3 independent mRNA samples per sgRNA, error bars indicate ± 1 SD. \*p < 0.05 and \*\*p < 0.01 (unpaired two-tailed t test, equal variances).  
 (C) *PMAIP1*-targeting sgRNAs specifically enrich during CRISPR screen in hESC but not cancer cell lines. The x axis plots CRISPR screens conducted in

(Figure 4C; Table S7). As expected, multiple sgRNAs targeting *ROCK1* and *MYH9*, the genetic targets of ROCK inhibitors and blebbistatin, were recovered. Myosin is a hexameric motor protein that is composed of six subunits with three subtypes. The screen recovered three sgRNAs for *MYH9*, a myosin heavy chain, five sgRNAs for *MYL6*, a non-phosphorylated myosin light chain, and two sgRNAs for the ROCK target *MYL9/MLC2*, a phosphorylated myosin light chain. There are many myosin proteins, but our screen identified three of five of the most abundantly expressed in hPSCs (Figure 4B). This reiterates the importance of myosin activation in membrane blebbing and dissociation-induced death. A number of additional genes have roles in the actin and myosin network or cytoskeleton, including *DAPK3*, *PAWR*, *OPHN1*, *FLII*, and *KIF3A* (Figure 4D). Overall STRINGdb analysis detected a connected set of genes with ties to the actin and myosin regulatory network (Figure 4D). In general members of this network did not enrich during the fitness screen, suggesting that they specifically regulate dissociation-induced death and not fitness (Figure 4E).

### ***PAWR* Is Required for Dissociation-Induced Death**

For follow-up studies, we focused on the strongest hit from the screen, the pro-apoptotic regulator *PAWR* (Hebbar et al., 2012). *PAWR* has no known biological role in the early embryo or during dissociation-induced death of hPSCs. The screen recovered all five sgRNAs targeting *PAWR* in the genome-scale library, and the barcode reads were highly abundant (Figure 4C). Unlike sgRNAs for the *TP53* pathway that enrich throughout the CRISPR screen, *PAWR* and *MYL6* have no effect on fitness in the presence of thiazovivin (Figure 4E). We repeated the results using three independent lentiCRISPRs to knock out *PAWR* in iCas9 expressing H1-hESC cells. *PAWR* mutants are able to survive without thiazovivin, while control cells do not (Figure S4). To independently validate these results, we used CRISPR-mediated interference (CRISPRi) to knock down the expression of *PAWR* mRNA without causing DNA damage or genetic mutations (Data S1) (Qi et al., 2013). By using a H1-hESC line constitutively expressing dCas9 fused to a KRAB domain and sgRNAs targeting *PAWR* promoter, we also detected an increase in the survival of dissociated cells in the absence of thiazovivin (Figure S4).

H1-hESC lines and 14 additional transformed lines. Five independent sgRNAs marked by dots. The y axis represents log<sub>2</sub>(fold change).

(D) *PMAIP1* mutant hPSCs are insensitive to DNA damage. Live imaging of confluence in *MAPT* sgRNA expressing iCas9 cells ± DSB (+dox/Cas9) in control or *PMAIP1*<sup>-/-</sup> knockout cell line. Unlike DSB-treated control cells, the *PMAIP1*<sup>-/-</sup> mutants survive in the presence of DSBs. Black lines indicate control and magenta lines indicate *PMAIP1*<sup>-/-</sup> mutants. Solid lines are without dox, and dashed lines are cultured with dox. The y axis is percentage confluency each point represents mean (four images per well, n = 3 wells). Error bars indicate ± 1 SD. The x axis depicts time in days of treatment.

(E) qPCR of *TP53* target genes indicates *PMAIP1* functions downstream of *TP53*. *P21* and *FAS* mRNA is induced by *MAPT* targeting sgRNAs in iCas9 control cells 2 days after dox treatment. *PMAIP1*<sup>-/-</sup> mutants exhibit increased levels of *P21* and *FAS* mRNA, which is absent in *TP53*<sup>-/-</sup> mutants. The y axis is relative expression is calculated by comparing the *MAPT* targeting sgRNA plus (+dox) or minus Cas9 expression (-dox). \*p < 0.05, \*\*p < 0.01, \*\*\*p < 0.001, and \*\*\*\*p < 0.0001 (unpaired two-tailed t test, equal variances). Error bars ± 1 SD. See also Figures S1, S3, and S5.



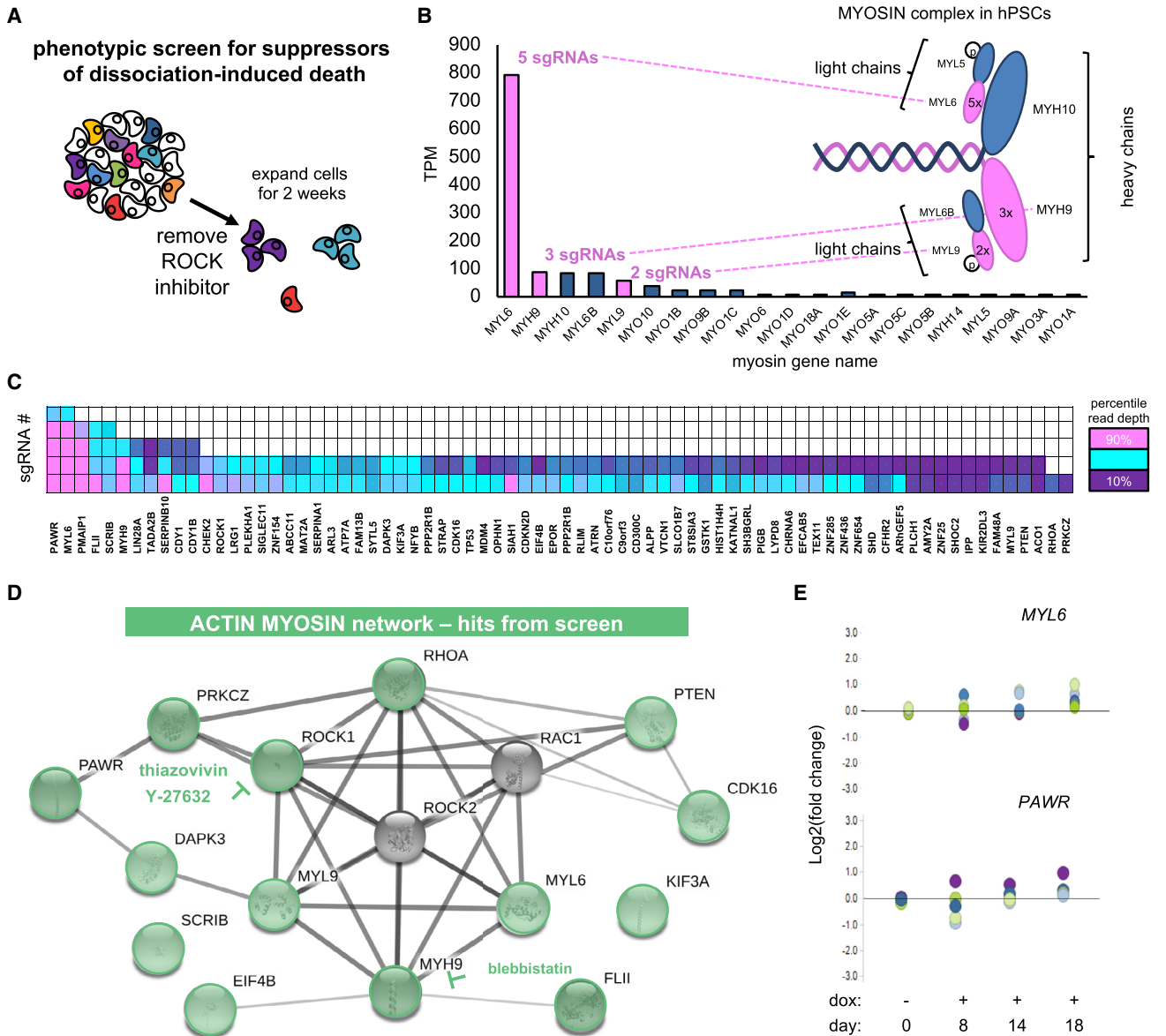


**Figure 4. Genetic Screen for Suppressors of Dissociation-Induced Death**

(A) Diagram depicting screen shows the dissociation and replating of the genome-scale mutant cell library without thiazovivin (a ROCK inhibitor). Most cells did not survive the treatment; however, at the end of 2 weeks, some large colonies were recovered for DNA isolation and NGS analysis.

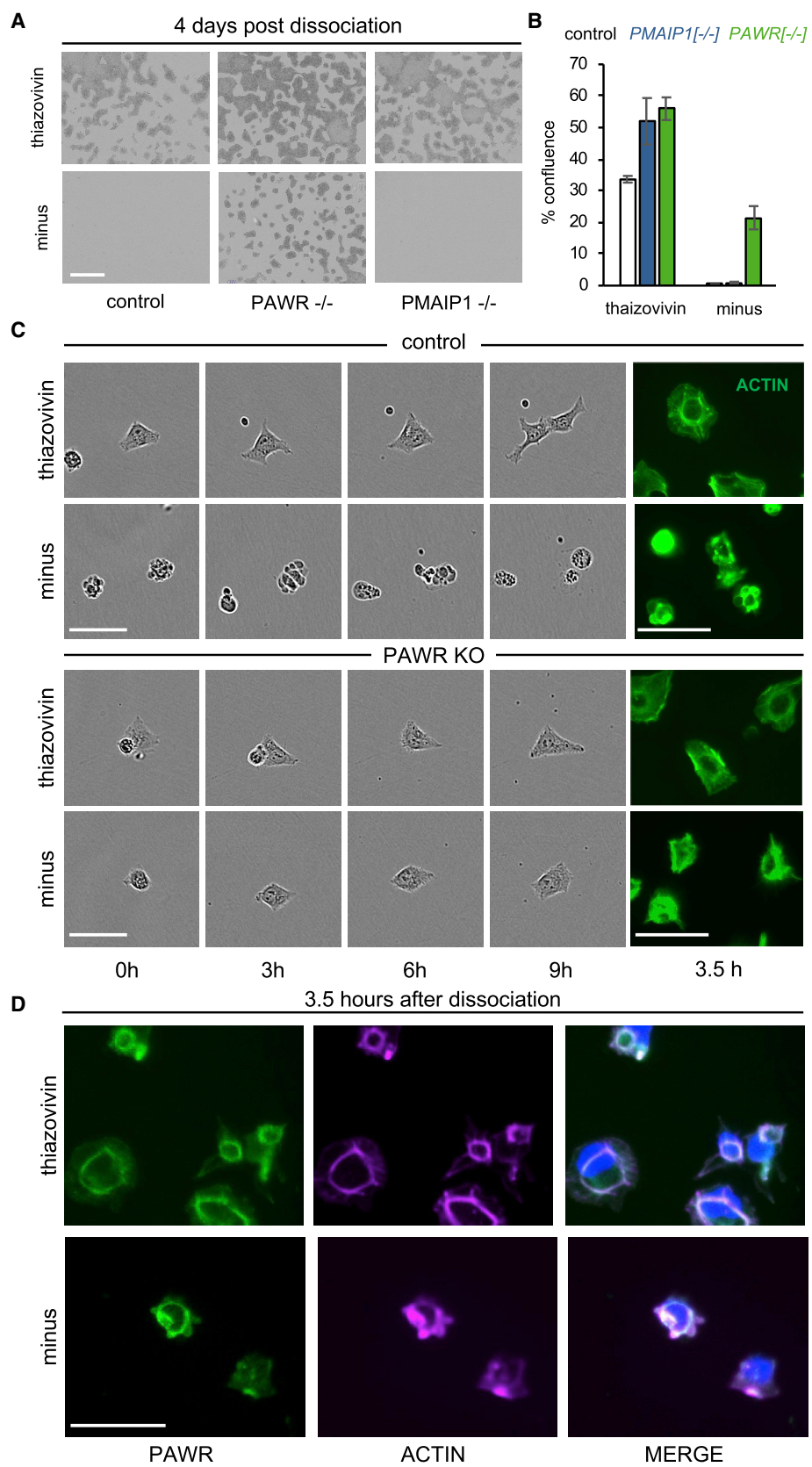
(B) The screen recovered three of six subunits of the hexameric myosin motor protein that regulates blebbing in hPSCs. The y axis depicts average TPM in H1-hESC. The x axis depicts myosin genes expressed >1 TPM in H1-hESCs. Myosin genes recovered by screen in pink. Genes that were not detected by screen are in blue.

(C) Heatmap depicting number of sgRNAs recovered on the y axis and each gene on the x axis. Colors indicate the abundance of each sgRNA recovered. Pink marks greater than 90th percentile, and purple marks less than 10th percentile.

(D) STRINGdb analysis highlights actin and myosin gene network among mutations that allow cells to survive dissociation in the absence of ROCK inhibitors. Hits from screen marked in green.

(E) *MYL6* and *PAWR* specifically regulate survival after dissociation and do not enrich during CRISPR screen. Each dot represents five independent sgRNAs per gene, and NGS quantifies representation of lentiCRISPRs infected cells. Samples were normalized to the day 0 population and y axis represents  $\log_2$ (fold change). Day 0 data shown is from freeze and thaw samples maintained at 2,700x. The x axis plots each condition over time. Cas9+ samples were treated with dox to induce Cas9 expression.

See also Figures S1, S4, and S6.



(legend on next page)

To conduct detailed analysis of *PAWR* mutants, we exposed cells to Cas9 and sgRNAs targeting *PAWR* and generated a knockout cell line with a normal karyotype (Figure S4). The suppression of dissociation-induced death is specific to *PAWR* mutants, as *PMAIP1* mutants are unable to survive passaging without thiazovivin (Figures 5A and 5B). Conversely, *PAWR* mutants are unable to survive DSB-induced toxicity, further demonstrating the specificity of the respective phenotypes (Figure S4E). We next examined how *PAWR* mutants survive by time-lapse microscopy. After single-cell dissociation, control cells without thiazovivin exhibit membrane blebbing and subsequently die (Figure 5C). Conversely, *PAWR* mutants without thiazovivin have greatly reduced blebbing and survive as single cells by extending cell projections, which promote attachment and survival (Figure 5C). We further examined cytoskeletal organization using phalloidin to stain filamentous (F) actin. The thiazovivin-treated cells have an increased surface area, a fanned-out shape with actin stress fibers, and a large circular adhesion belt-like structure (Figure 5C). In the absence of thiazovivin, control cells have many small actin rings that mark membrane blebs. *PAWR* mutants without thiazovivin exhibit reduced membrane blebbing and small actin rings (Figure 5C).

Molecularly, *PAWR* has dual roles as a transcriptional repressor that causes cell death and as an actin-binding protein that regulates contractility (Johnstone et al., 1996; Burikhanov et al., 2009; Vetterkind and Morgan, 2009). Despite having abundant *PAWR* mRNA, *PAWR* protein is post-transcriptionally regulated and induced by dissociation in hPSCs (Figures S4 and S5). Immunofluorescence did not detect *PAWR* protein in the nucleus; however, we did observe localization of *PAWR* with F-actin in both thiazovivin-treated and untreated cells (Figure 5D). *PAWR* localized to adhesion belt-like structures in the presence of thiazovivin and to membrane blebs in the untreated cells after dissociation. Additional hits from the screen, *PRKCZ* and *SCRIB*, also localized to membrane blebs (Figure S6). Both *PRKCZ* and *SCRIB* are expressed in the early mouse embryo and exhibit a ROCK-dependent cell polarity (Kono et al., 2014). Cumulatively, we have identified a role for *PAWR* in dissociation-induced death. *PAWR* mutants survive dissociation without ROCK inhibitors because of a failure to initiate membrane blebbing and downstream caspase activation (Figure S5) (Ohgushi et al., 2010). Furthermore, *PAWR* is a known pro-apoptotic factor, and we

have demonstrated that *PAWR* protein is induced upon dissociation and colocalizes with the actin network that is responsible for initiating membrane blebbing and subsequent cell death.

### FACS-Based Screen for Regulators of Pluripotency

Although our fitness screen detected a significant hPSC-specific dropout of *OCT4*, other critical regulators of pluripotency such as *NANOG* did not affect fitness (Figure 1E; Table S4). A genome-scale fitness screen in mouse embryonic stem cells (mESCs) had similar results and reported the dropout of only three genes regulating blastocyst development (Koike-Yusa et al., 2014). Pluripotency and cellular fitness of hPSCs may not be related, and this indicates that some differentiated cell types may not exhibit changes in fitness when cultured in the pluripotent media. To specifically identify regulators of human pluripotency, we conducted a FACS-based pooled screen using an *OCT4* antibody. One year after conducting the first screen, we thawed a genome-scale CRISPR cell library (–dox) and expanded the cells prior to conducting the screen (Figure S1). The cells were mutagenized with Cas9 for 8 days prior to FACS to collect cells with high (*OCT4*<sup>HIGH</sup>) and low (*OCT4*<sup>LOW</sup>) *OCT4* expression (Figure 6A). Log<sub>2</sub>(fold change) was calculated by comparing the *OCT4*<sup>LOW</sup> group with the *OCT4*<sup>HIGH</sup> group. We plotted the p values calculated by the RSA test against Q1- and Q3-based Z scores for *OCT4*<sup>LOW</sup> and *OCT4*<sup>HIGH</sup>, respectively (Figure 7B; Table S8). Importantly, we detected a significant enrichment of *OCT4* and *NANOG* targeting sgRNAs in the *OCT4*<sup>LOW</sup> group. We also detected an enrichment of *TGFBR1/2* genes required to maintain the culture of hPSCs and the chromatin regulators *EP300* and *SMARCA4/BRG1*, which regulate *OCT4* expression and function in hPSCs (Singhal et al., 2010; Chen et al., 2011; Wang et al., 2012; King and Klose, 2017). Using STRINGdb, we identified a core network of genes connected to *OCT4* in the *OCT4*<sup>LOW</sup> group (Figure 6C). This highlights the ability of phenotypic CRISPR screening to identify relevant gene networks. Additionally, the *OCT4*<sup>HIGH</sup> group identified factors that promote differentiation, such as *HAND1*, *KDM5B*, and *EIF4G2* (Table S8) (Yamanaka et al., 2000; Hough et al., 2006; Kidder et al., 2013). Many of the genes in these lists have published roles in regulating pluripotency, reprogramming or embryonic development, and further investigation of the less studied genes will reveal insights into the human pluripotent state (Tables S8 and S9).

### Figure 5. *PAWR* Is Required for Dissociation-Induced Death

(A) *PAWR* mutants survive single-cell dissociation in the absence of thiazovivin (a ROCK inhibitor) treatment. Control cells and *PMAIP1* knockout do not survive without thiazovivin treatment. Bright-field images taken of live iCas9 cells 4 days after dissociation. Scale bar, 800  $\mu$ M.

(B) Quantification of survival in the presence or absence of thiazovivin. Percentage confluence was measured 4 days after replating in control, *PAWR* knockout, and *PMAIP1* knockout cells. Bars represent mean from three independent wells with four images per well. Error bars indicate  $\pm 1$  SD from four images per well from three independent wells. The dissociation-induced survival of *PAWR* mutant hPSCs was replicated more than three times.

(C) Time-lapse microscopy of live cells during first 9 h of replating. Control and *PAWR* knockout hPSCs survive replating in the presence of thiazovivin by extending cellular projections and forming an actin adhesion belt organized with stress fibers. Phalloidin stain at 3.5 h in fixed cells. Control cells without thiazovivin have abundant membrane blebbing, and this is highlighted by the presence of small circular actin rings in phalloidin stained cells. *PAWR* mutants have reduced blebbing and intermediate phalloidin staining without small actin rings. Scale bar, 50  $\mu$ M.

(D) Immunofluorescence detects *PAWR* protein colocalizing with F-actin. Following dissociation, *PAWR* protein colocalizes with F-actin in the presence of thiazovivin in adhesion belt-like structures and in the absence of thiazovivin in membrane blebs. Green indicates *PAWR* protein. Magenta indicates phalloidin-stained F-actin. Blue indicates DAPI-stained nuclei. Scale bar, 50  $\mu$ M.

See also Figures S1, S4, and S5.

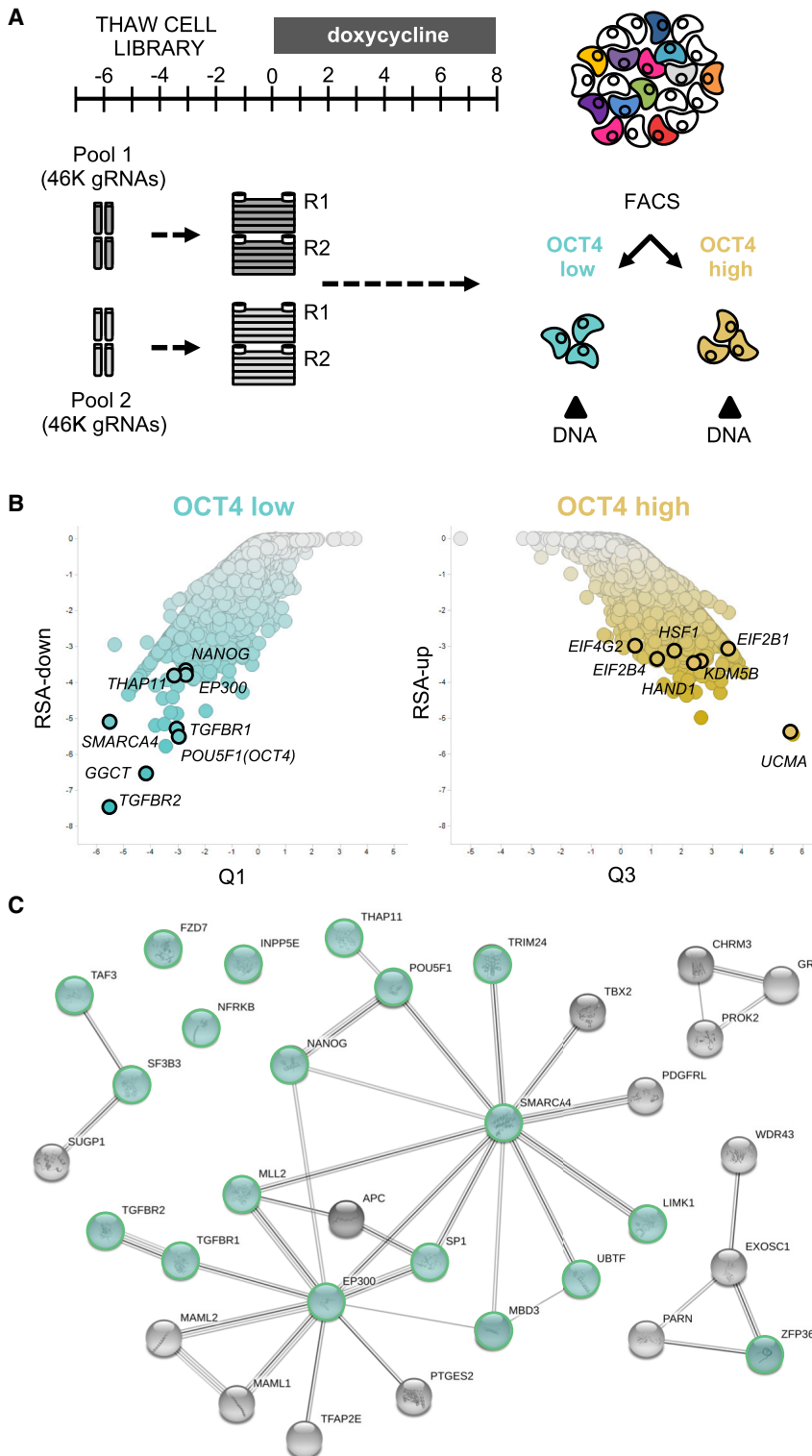


**Figure 6. OCT4 FACS-Based Screen Identifies Pluripotency Gene Network**

(A) Diagram depicting FACS-based CRISPR screen using an OCT4 specific antibody to sort OCT4 high- and low-expressing cells. Cells were mutagenized with Cas9 for 8 days prior to FACS sorting, and DNA isolation and NGS were used to identify enrichment of sgRNAs in the high- and low-OCT4 populations.

(B) Scatterplot depicting gene level results for genome-scale OCT4 FACS screen. Green depicts OCT4<sup>LOW</sup> and gold depicts OCT4<sup>HIGH</sup> enriched sgRNAs. The y axis is a p value generated from RSA down and up analysis. The x axis marks the Z score (Q1/Q3).

(C) STRINGdb analysis identifies a 20-gene network connected to OCT4 among gene sgRNAs that were enriched in cells with low OCT4 protein. Genes with published roles in pluripotency, reprogramming, and embryo development are highlighted in green. See also Figure S1.

ever, the static state of these cells has revealed less about genes with developmental functions (Hart et al., 2015). To compare hPSC results to cancer cell lines, we conducted pairwise Pearson correlation coefficients using Bayes factor distributions (cancer data from Hart et al., 2015). The analysis revealed that hPSCs formed a distinct cluster (Figure 7A) and is consistent with the partial overlap between core-essential genes in cancer and fitness genes in hPSCs (52%; Figure 1E). To focus on gene networks specific to hPSCs, we conducted bioinformatics analysis comparing 829 core-essential cancer genes (essential for five of five cell lines; Hart et al., 2015) with hPSC-specific gene sets identified by our screens. A total of 661 hPSC-specific genes were obtained from the fitness screen (365 depleted and 20 enriched p53-related genes), dissociation-induced death screen (76), and the OCT4 FACS screen (212) (Table S10). The gene lists were analyzed using the PANTHER classification system (pantherdb.org). PANTHER pathway analysis identified a greater diversity of 92 enriched pathways in hPSCs and only 38 in the cancer lines (Figure 7B). In accordance with this, we also detected an increase in the number of genes with receptor and signal transducer activity molecular functions (Figure 7C). The hPSC-enriched pathways included several expected regulators: FGF, TGF-beta, and WNT (Figure 7B). FGF2 and TGFβ are critical components of E8 media and are required to maintain

### Identification of hPSC-Specific Fitness and Pluripotency Gene Networks

Extensive CRISPR screening in cancer cell lines has provided a wealth of knowledge about their genetic dependencies. How-



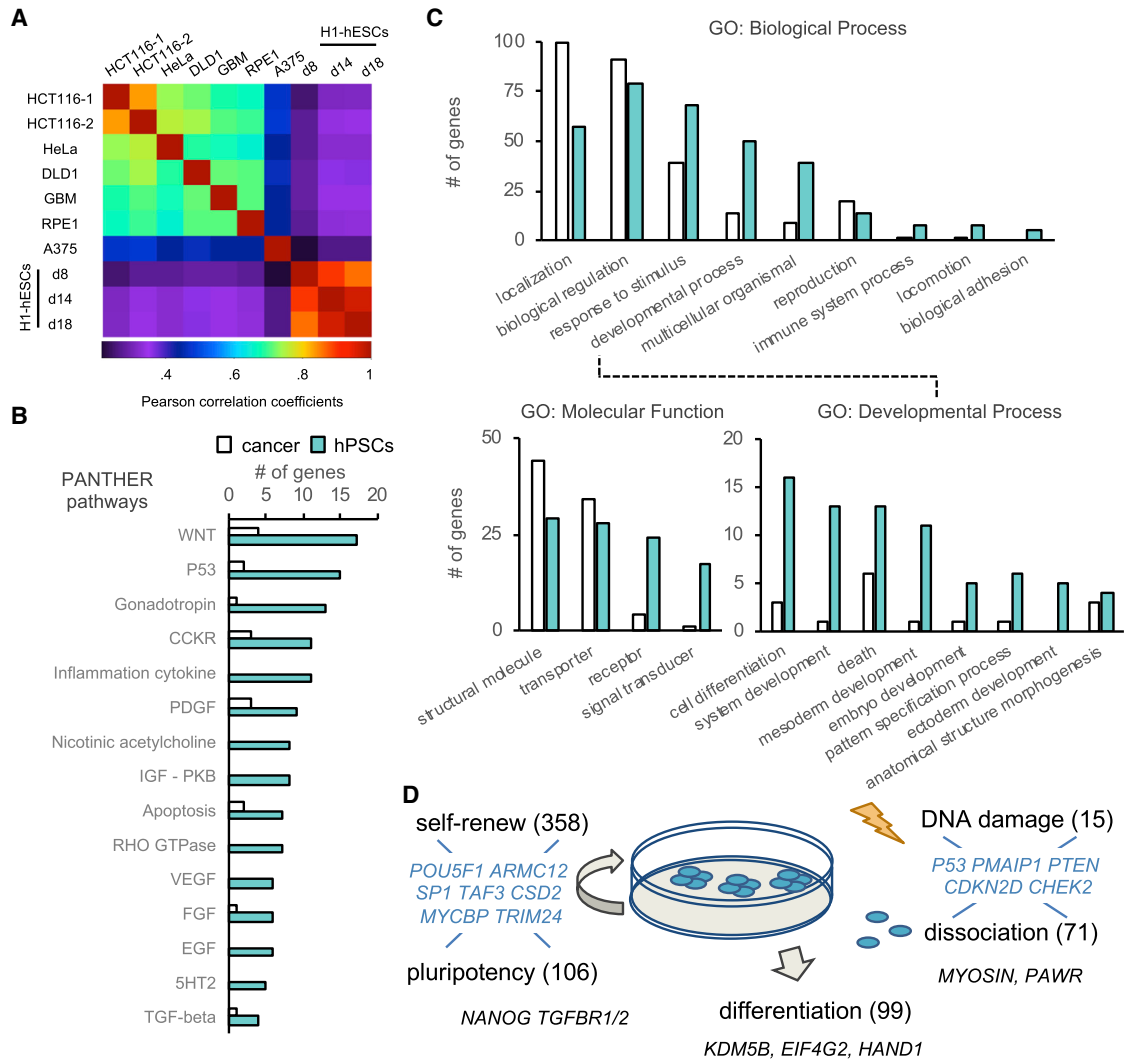


### Figure 7. Identification of hPSC-Specific Essential Gene Networks

(A) Heatmap of Pearson correlation coefficients adapted from [Hart et al. \(2015\)](#) to include CRISPR screening data in H1-hESCs.

(B) PANTHER pathway analysis identified 92 enriched pathways in hPSCs. A subset of 15 hPSC-specific pathways are depicted.

(C) Depiction of Gene Ontology categories including biological processes, molecular functions, and developmental processes that are specific to hPSCs but not cancer cell lines.

(D) Schematic of genes identified by CRISPR screening in hPSCs and their putative functions. Seven hundred seventy fitness genes regulate the self-renewing potential of hPSCs. One hundred thirteen genes with low OCT4 protein are implicated in pluripotency, and 99 genes with increased OCT4 protein may promote differentiation. Twenty genes are implicated in the toxic response to DNA damage. Seventy-six genes are implicated in the sensitivity of hPSCs to single-cell dissociation. (B–D) Bioinformatic analysis of 829 core-essential cancer (white bars; [Hart et al., 2015](#)) and 653 hPSC-specific genes (green bars). Genes in multiple categories are shown in blue. See also [Figure S1](#).

pluripotency *in vitro* ([Chen et al., 2011](#)). WNT signaling regulates both differentiation and pluripotency in ESCs ([Sokol, 2011](#)). Activation of EGF, PDGF, and VEGF is also important for the maintenance of the pluripotent state in ([Brill et al., 2009](#)). P53 and CCKR/Rho GTPases pathways, which regulate apoptosis and have critical roles in determining the sensitivity of hPSCs to DNA damage and enzymatic dissociation, were also enriched ([Figure 7B](#)). Examination of the biological processes' gene ontology revealed an increase in the number of development

and multicellular organism genes ([Figure 7C](#)). Furthermore, sub-dividing the developmental process category revealed enrichment of genes regulating cell death, differentiation, and early developmental stages ([Figure 7C](#)). Globally these results highlight the identification of cell type-specific genes regulating different aspects of the pluripotent state. By screening for regulators of three fundamental processes governing the culture of hPSCs, we have successfully identified known regulators in addition to a plethora of genes involved in stem cell biology

(Figure 7D). These genes are a blueprint for human pluripotency and will serve as a useful resource for the human development and stem cell communities.

## DISCUSSION

The use of hPSCs in large-scale functional genomics studies has been limited by technical constraints. Prior to our study, it was unclear that genome-scale CRISPR screens were possible in hPSCs, as the first attempts had poor performance (Hart et al., 2014; Shalem et al., 2014). We overcame this by building a high-performance two-component CRISPR/CAS9 system for hPSCs. The performance, across many sgRNAs, made the platform amenable to high-throughput screening. Using iCas9 in hPSCs it is possible to perturb hundreds of genes in arrayed format or the entire genome in pooled format. The system is renewable, and a pool of stem cells with sgRNAs to the entire genome can be banked, distributed, and used for successive screens in hPSCs and their differentiated progeny. Beyond technical proficiency, we identified genes that regulate fundamental stem cell processes such as self-renewal, their inherent sensitivity to DNA damage, single-cell cloning, pluripotency, and differentiation.

First, we identified 770 genes required for the self-renewal of hPSC. A majority of these genes have established roles in fitness, while 365 of these genes are specific to hPSCs. This set of genes could be used to inform a systematic approach to improve the consistency, robustness, and user-friendliness of hPSC culture conditions. During the fitness screen, we also determined that Cas9 activity imposes selective pressure on DNA damage-sensitive hPSCs. This caused the enrichment of 20 genes that are connected to *TP53*. Consistent with this, dominant-negative *TP53* mutations and deletions recurrently occur and provide a selective advantage during the culture of hPSCs (Amir et al., 2017; Merkle et al., 2017). In addition to *TP53*, we identified a hPSC-specific role for *PMAIP1* in determining the extreme sensitivity of hPSCs to DNA damage. Like *TP53*, deletions of chromosome 18 spanning the *PMAIP1* locus have been recurrently observed during hPSC culture (Amps et al., 2011) and suggest that *PMAIP1* deletion may be responsible for enhanced survival of these lines. These *TP53*-related genes have the potential to improve the efficiency or safety of genome engineering through transient inhibition or by monitoring their spontaneous mutation rate during hPSC culture (Merkle et al., 2017; Ihry et al., 2018).

Second, we identified 76 genes that enhance the survival of hPSCs during single-cell dissociation. Collectively, the screen uncovered an actin and myosin network required for membrane blebbing and cell death caused by dissociation. We identified a role for *PAWR*, a pro-apoptotic regulator that is induced upon dissociation. *PAWR* is required for membrane blebbing and subsequent death of dissociated hPSCs in the absence of ROCK inhibitors. Importantly, the results are developmentally relevant, and we also identified *SCRIB* and *PRKCZ*, which are known regulators of cell polarity in the early mouse embryo (Kono et al., 2014). *PAWR* has been shown to physically interact with *PRKCZ* and suggests a potential link between cell polarity and dissociation-induced death (Díaz-Meco et al., 1996). These hits appear to

be related to the polarized epiblast-like state of primed hPSC and could explain why polarized hPSCs are sensitive to dissociation, whereas unpolarized naive mESCs are not (Takashima et al., 2015). Last, this set of genes could enable focused approaches to improve the single-cell cloning efficiencies of hPSCs and the culture of naive hPSCs.

In the final screen, by subjecting our hPSC CRISPR library to FACS sorting on OCT4 protein, we identified 113 genes that are required to maintain pluripotency and 99 genes that potentially regulate differentiation. Overall, the screen identified an entire network of genes related to OCT4. Nineteen of these genes have previously indicated roles in pluripotency, embryo development, and reprogramming (Table S9). Future studies on the genes in the list will yield new insights about the genetic control of pluripotency and differentiation. These gene sets could guide rational improvements to protocols for the maintenance, differentiation, and reprogramming of hPSCs.

Overall, the results highlight the ability of unbiased genome-scale screens to identify critical and regulators of hPSC biology. Importantly, some of the strongest hits, such as *PAWR* and *PMAIP1*, were also identified in haploid hPSC screens (Yilmaz et al., 2018). Future investigation into the genes provided by these screens will be a step toward the genetic dissection of the human pluripotent state. Herein we provide simple and scalable work flows that will lower the entry barrier for additional labs to conduct large-scale CRISPR screens in hPSCs. The scalable and bankable platform described here is a renewable resource that will allow successive screens and the distribution of CRISPR-infected hPSC libraries. We anticipate that the use of CRISPRi will improve the performance. Reducing Cas9-induced toxicity will limit artifacts and reduce need for high library coverage and costs to enable systematic screening in many independent hPSC lines and differentiated cell types. The platform could potentially be used to improve the generation, culture, and differentiation capacity of hPSCs. It can be applied to the study of development and disease in wide variety of differentiated cell types. Established protocols for neurons, astrocytes, cardiomyocytes, hepatocytes, and beta cells can be exploited to dissect the genetic nature of development and homeostasis in disease-relevant cell types. This resource opens the door for the systematic genetic dissection of disease-relevant human cells in way that was only before possible in model organisms.

## STAR★METHODS

Detailed methods are provided in the online version of this paper and include the following:

- KEY RESOURCES TABLE
- CONTACT FOR REAGENT AND RESOURCE SHARING
- EXPERIMENTAL MODEL AND SUBJECT DETAILS
  - Human Pluripotent Stem Cell lines
  - Large-scale culture of hPSCs
- METHOD DETAILS
  - Genome Engineering
  - lentiCRISPR packaging
  - Large-scale transduction of hPSCs

- Banking lentiCRISPR infected hPSC library
- Pooled Mutagenesis (CRISPR nuclease/interference)
- CRISPR nuclease
- CRISPR interference
- OCT4 FACS-BASED screen
- DNA isolation and NGS libraries
- mRNA expression
- Assaying sensitivity to DNA damage
- Assaying survival without ROCK inhibitor
- Immunofluorescence and Western Blotting
- Primary antibodies
- Secondary Antibodies
- **QUANTIFICATION AND STATISTIC ANALYSIS**
  - Figures 1B and 7A
  - Figures 1D, 2A, and 6B
  - Figure 1E
  - Figures 3B and 3E
  - Figure 3A and S4F
- **DATA AND SOFTWARE AVAILABILITY**

#### SUPPLEMENTAL INFORMATION

Supplemental Information can be found online at <https://doi.org/10.1016/j.celrep.2019.03.043>.

#### ACKNOWLEDGMENTS

We would like to thank R. Maher, J. Alford, S. An, and D. Shkzoza for their support with sgRNA cloning. We would like to thank Arti Patel for help with western blotting. We would like to thank F. Cong, W. Forrester, and L. Murphy for access to *PMAIP1* pooled screening results in cancer cell lines. We thank Jason Moffat and Barbara Mair for the open discussion related to this research. All research was funded by the Novartis Institutes for Biomedical Research.

#### AUTHOR CONTRIBUTIONS

R.J.I. and A.K. designed all experiments and wrote the manuscript. M.R.S., K.A.W., and R.D. revised the manuscript. R.J.I. conducted live cell imaging, immunofluorescence, qPCR, and western blotting. S.K. and K.A.W. generated Ngn2-inducible cell lines and differentiated them into Ngn2 neurons. M.S. helped with genome-scale hPSC culture, packaged lentiviral sgRNAs, and generated CRISPRi lines. B.H. conducted *PAWR* knockdowns in human dermal fibroblast (hDFN) CRISPRi iPSC line. Q.W. packaged genome-wide lentiviral supernatants. E.F. prepped DNA samples for NGS. J.R. sequenced CRISPR indels. R.C.A. generated precision recall values using the BAGEL algorithm. S.K. generated RNA expression data in hPSCs and NGN2 neurons, and these data were analyzed by R.R. G.R.H., Z.Y., and G.M. helped design the pooled screen and performed the analysis. J.S.R.-H. generated sgRNA libraries. C.R. sequenced pooled fitness screen samples. S.P. sorted OCT4-high- and OCT4-low-expressing cells by FACS. C.Y. and D.J.H. sequenced and analyzed the OCT4 FACS screen.

#### DECLARATION OF INTERESTS

All authors were employees of the Novartis Institutes for Biomedical Research at the time this research was conducted. R.J.I. and A.K. are inventors on patent applications related to this work.

Received: May 18, 2018

Revised: December 20, 2018

Accepted: March 13, 2019

Published: April 9, 2019

#### REFERENCES

- Aguirre, A.J., Meyers, R.M., Weir, B.A., Vazquez, F., Zhang, C.-Z., Ben-David, U., Cook, A., Ha, G., Harrington, W.F., Doshi, M.B., et al. (2016). Genomic copy number dictates a gene-independent cell response to CRISPR-Cas9 targeting. *Cancer Discov.* 6, 914–929.
- Amir, H., Touboul, T., Sabatini, K., Chhabra, D., Garitaonandia, I., Loring, J.F., Morey, R., and Laurent, L.C. (2017). Spontaneous single-copy loss of TP53 in human embryonic stem cells markedly increases cell proliferation and survival. *Stem Cells* 35, 872–885.
- Amps, K., Andrews, P.W., Anyfantis, G., Armstrong, L., Avery, S., Baharvand, H., Baker, J., Baker, D., Munoz, M.B., Beil, S., et al.; International Stem Cell Initiative (2011). Screening ethnically diverse human embryonic stem cells identifies a chromosome 20 minimal amplicon conferring growth advantage. *Nat. Biotechnol.* 29, 1132–1144.
- Anders, S., Pyl, P.T., and Huber, W. (2015). HTSeq—a Python framework to work with high-throughput sequencing data. *Bioinformatics* 31, 166–169.
- Bidinosti, M., Botta, P., Krüttner, S., Proenca, C.C., Stoehr, N., Bernhard, M., Fruh, I., Mueller, M., Bonenfant, D., Voshol, H., et al. (2016). CLK2 inhibition ameliorates autistic features associated with SHANK3 deficiency. *Science* 357, 1199–1203.
- Brill, L.M., Xiong, W., Lee, K.-B., Ficarro, S.B., Crain, A., Xu, Y., Terskikh, A., Snyder, E.Y., and Ding, S. (2009). Phosphoproteomic analysis of human embryonic stem cells. *Cell Stem Cell* 5, 204–213.
- Burikhanov, R., Zhao, Y., Goswami, A., Qiu, S., Schwarze, S.R., and Rangnekar, V.M. (2009). The tumor suppressor Par-4 activates an extrinsic pathway for apoptosis. *Cell* 138, 377–388.
- Chambers, I., Silva, J., Colby, D., Nichols, J., Nijmeijer, B., Robertson, M., Vrana, J., Jones, K., Grotewold, L., and Smith, A. (2007). Nanog safeguards pluripotency and mediates germline development. *Nature* 450, 1230–1234.
- Chen, G., Hou, Z., Gulbranson, D.R., and Thomson, J.A. (2010). Actin-myosin contractility is responsible for the reduced viability of dissociated human embryonic stem cells. *Cell Stem Cell* 7, 240–248.
- Chen, G., Gulbranson, D.R., Hou, Z., Bolin, J.M., Ruotti, V., Probasco, M.D., Smuga-Otto, K., Howden, S.E., Diol, N.R., Propson, N.E., et al. (2011). Chemically defined conditions for human iPSC derivation and culture. *Nat. Methods* 8, 424–429.
- Chia, N.Y., Chan, Y.S., Feng, B., Lu, X., Orlov, Y.L., Moreau, D., Kumar, P., Yang, L., Jiang, J., Lau, M.S., et al. (2010). A genome-wide RNAi screen reveals determinants of human embryonic stem cell identity. *Nature* 468, 316–320.
- Cong, L., Ran, F.A., Cox, D., Lin, S., Barretto, R., Habib, N., Hsu, P.D., Wu, X., Jiang, W., Marraffini, L.A., and Zhang, F. (2013). Multiplex genome engineering using CRISPR/Cas systems. *Science* 339, 819–823.
- DasGupta, R., Kaykas, A., Moon, R., and Perrimon, N. (2005). Functional genomic analysis of the Wnt-wingless signaling pathway. *Science* 308, 826–833.
- DeJesus, R., Moretti, F., McAllister, G., Wang, Z., Bergman, P., Liu, S., Frias, E., Alford, J., Reece-Hoyes, J.S., Lindeman, A., et al. (2016). Functional CRISPR screening identifies the ufmylation pathway as a regulator of SQSTM1/p62. *Elife* 5, e17290.
- Díaz-Meco, M.T., Municio, M.M., Frutos, S., Sanchez, P., Lozano, J., Sanz, L., and Moscat, J. (1996). The product of par-4, a gene induced during apoptosis, interacts selectively with the atypical isoforms of protein kinase C. *Cell* 86, 777–786.
- Dobin, A., Davis, C.A., Schlesinger, F., Drenkow, J., Zaleski, C., Jha, S., Batut, P., Chaisson, M., and Gingeras, T.R. (2013). STAR: ultrafast universal RNA-seq aligner. *Bioinformatics* 29, 15–21.
- Echeverri, C.J., Beachy, P.A., Baum, B., Boutros, M., Buchholz, F., Chanda, S.K., Downward, J., Ellenberg, J., Fraser, A.G., Hacohen, N., et al. (2006). Minimizing the risk of reporting false positives in large-scale RNAi screens. *Nat. Methods* 3, 777–779.

- Gutekunst, M., Mueller, T., Weilbacher, A., Dengler, M.A., Bedke, J., Kruck, S., Oren, M., Aulitzky, W.E., and van der Kuip, H. (2013). Cisplatin hypersensitivity of testicular germ cell tumors is determined by high constitutive Noxa levels mediated by Oct-4. *Cancer Res.* **73**, 1460–1469.
- Haapaniemi, E., Botla, S., Persson, J., Schmierer, B., and Taipale, J. (2017). Inhibition of p53 improves CRISPR/Cas-mediated precision genome editing. *Main text. bioRxiv.* <https://doi.org/10.1101/180943>.
- Hart, T., and Moffat, J. (2016). BAGEL: a computational framework for identifying essential genes from pooled library screens. *BMC Bioinformatics* **17**, 164.
- Hart, T., Brown, K.R., Sircoulomb, F., Rottapel, R., and Moffat, J. (2014). Measuring error rates in genomic perturbation screens: gold standards for human functional genomics. *Mol. Syst. Biol.* **10**, 733.
- Hart, T., Chandrashekar, M., Aregger, M., Durocher, D., Angers, S., Moffat, J., Crispr, H., Hart, T., Chandrashekar, M., Aregger, M., et al. (2015). High-resolution CRISPR screens reveal fitness genes and genotype-specific cancer liabilities. *Cell* **163**, 1515–1526.
- Hebbbar, N., Wang, C., and Rangnekar, V.M. (2012). Mechanisms of apoptosis by the tumor suppressor Par-4. *J. Cell. Physiol.* **227**, 3715–3721.
- Hough, S.R., Clements, I., Welch, P.J., and Wiederholt, K.A. (2006). Differentiation of mouse embryonic stem cells after RNA interference-mediated silencing of OCT4 and Nanog. *Stem Cells* **24**, 1467–1475.
- Ihry, R.J., Worringer, K.A., Salick, M.R., Frias, E., Ho, D., Theriault, K., Kommneni, S., Chen, J., Sondey, M., Ye, C., et al. (2018). p53 inhibits CRISPR-Cas9 engineering in human pluripotent stem cells. *Nat. Med.* **24**, 939–946.
- Jinek, M., Chylinski, K., Fonfara, I., Hauer, M., Doudna, J.A., and Charpentier, E. (2012). A programmable dual-RNA-guided DNA endonuclease in adaptive bacterial immunity. *Science* **337**, 816–821.
- Johnstone, R.W., See, R.H., Sells, S.F., Wang, J., Muthukkumar, S., Englert, C., Haber, D.A., Licht, J.D., Sugrue, S.P., Roberts, T., et al. (1996). A novel repressor, par-4, modulates transcription and growth suppression functions of the Wilms' tumor suppressor WT1. *Mol. Cell. Biol.* **16**, 6945–6956.
- Kampmann, M., Horlbeck, M.A., Chen, Y., Tsai, J.C., Bassik, M.C., Gilbert, L.A., Villalta, J.E., Kwon, S.C., Chang, H., Kim, V.N., and Weissman, J.S. (2015). Next-generation libraries for robust RNA interference-based genome-wide screens. *Proc. Natl. Acad. Sci. U S A* **112**, E3384–E3391.
- Khandanpour, C., Phelan, J.D., Vassen, L., Schütte, J., Chen, R., Horman, S.R., Gaudreau, M.C., Krongold, J., Zhu, J., Paul, W.E., et al. (2013). Growth factor independence 1 antagonizes a p53-induced DNA damage response pathway in lymphoblastic leukemia. *Cancer Cell* **23**, 200–214.
- Kidder, B.L., Hu, G., Yu, Z.-X., Liu, C., and Zhao, K. (2013). Extended self-renewal and accelerated reprogramming in the absence of Kdm5b. *Mol. Cell. Biol.* **33**, 4793–4810.
- Kim, H., Rafiuddin-Shah, M., Tu, H.C., Jeffers, J.R., Zambetti, G.P., Hsieh, J.J.D., and Cheng, E.H.Y. (2006). Hierarchical regulation of mitochondrion-dependent apoptosis by BCL-2 subfamilies. *Nat. Cell Biol.* **8**, 1348–1358.
- King, H.W., and Klose, R.J. (2017). The pioneer factor OCT4 requires the chromatin remodeller BRG1 to support gene regulatory element function in mouse embryonic stem cells. *eLife* **6**, 1–24.
- Koike-Yusa, H., Li, Y., Tan, E.P., Velasco-Herrera, Mdel.C., and Yusa, K. (2014). Genome-wide recessive genetic screening in mammalian cells with a lentiviral CRISPR-guide RNA library. *Nat. Biotechnol.* **32**, 267–273.
- König, R., Chiang, C.Y., Tu, B.P., Yan, S.F., DeJesus, P.D., Romero, A., Bergauer, T., Orth, A., Krueger, U., Zhou, Y., and Chanda, S.K. (2007). A probability-based approach for the analysis of large-scale RNAi screens. *Nat. Methods* **4**, 847–849.
- Kono, K., Tamashiro, D.A.A., and Alarcon, V.B. (2014). Inhibition of RHO-ROCK signaling enhances ICM and suppresses TE characteristics through activation of Hippo signaling in the mouse blastocyst. *Dev. Biol.* **394**, 142–155.
- Langmead, B., and Salzberg, S.L. (2012). Fast gapped-read alignment with Bowtie 2. *Nat. Methods* **9**, 357–359.
- Laurent, L.C., Ulitsky, I., Slavin, I., Tran, H., Schork, A., Morey, R., Lynch, C., Harness, J.V., Lee, S., Barrero, M.J., et al. (2011). Dynamic changes in the copy number of pluripotency and cell proliferation genes in human ESCs and iPSCs during reprogramming and time in culture. *Cell Stem Cell* **8**, 106–118.
- Li, B., and Dewey, C.N. (2011). RSEM: accurate transcript quantifications from RNA-Seq data with or without a reference genome. *BMC Bioinformatics* **12**, 323.
- Love, M.I., Huber, W., and Anders, S. (2014). Moderated estimation of fold change and dispersion for RNA-seq data with DESeq2. *Genome Biol.* **15**, 550.
- Mali, P., Yang, L., Esvelt, K.M., Aach, J., Guell, M., DiCarlo, J.E., Norville, J.E., and Church, G.M. (2013). RNA-guided human genome engineering via Cas9. *Science* **339**, 823–826.
- Mallon, B.S., Chenoweth, J.G., Johnson, K.R., Hamilton, R.S., Tesar, P.J., Yavvatkar, A.S., Tyson, L.J., Park, K., Chen, K.G., Fann, Y.C., and McKay, R.D.G. (2013). StemCellDB: the human pluripotent stem cell database at the National Institutes of Health. *Stem Cell Res. (Amst.)* **10**, 57–66.
- Masui, S., Nakatake, Y., Toyooka, Y., Shimosato, D., Yagi, R., Takahashi, K., Okochi, H., Okuda, A., Matoba, R., Sharov, A.A., et al. (2007). Pluripotency governed by Sox2 via regulation of Oct3/4 expression in mouse embryonic stem cells. *Nat. Cell Biol.* **9**, 625–635.
- McDonald, E.R., 3rd, de Weck, A., Schlabach, M.R., Billy, E., Mavrikakis, K.J., Hoffman, G.R., Belur, D., Castelletti, D., Frias, E., Gampa, K., et al. (2017). Project DRIVE: a compendium of cancer dependencies and synthetic lethal relationships uncovered by large-scale, deep RNAi screening. *Cell* **170**, 577–592.e10.
- Merkle, F.T., Neuhausser, W.M., Santos, D., Valen, E., Gagnon, J.A., Maas, K., Sandoe, J., Schier, A.F., and Eggan, K. (2015). Efficient CRISPR-Cas9-mediated generation of knockin human pluripotent stem cells lacking undesired mutations at the targeted locus. *Cell Rep.* **11**, 875–883.
- Merkle, F.T., Ghosh, S., Kamitaki, N., Mitchell, J., Avior, Y., Mello, C., Kashin, S., Mekhoubad, S., Ilic, D., Charlton, M., et al. (2017). Human pluripotent stem cells recurrently acquire and expand dominant negative P53 mutations. *Nature* **545**, 229–233.
- Meyers, R.M., Bryan, J.G., McFarland, J.M., Weir, B.A., Sizemore, A.E., Xu, H., Dharia, N.V., Montgomery, P.G., Cowley, G.S., Pantel, S., et al. (2017). Computational correction of copy number effect improves specificity of CRISPR-Cas9 essentiality screens in cancer cells. *Nat. Genet.* **49**, 1779–1784.
- Munoz, D.M., Cassiani, P.J., Li, L., Billy, E., Korn, J.M., Jones, M.D., Golji, J., Ruddy, D.A., Yu, K., McAllister, G., et al. (2016). CRISPR screens provide a comprehensive assessment of cancer vulnerabilities but generate false-positive hits for highly amplified genomic regions. *Cancer Discov.* **6**, 900–913.
- Nichols, J., Zevnik, B., Anastasiadis, K., Niwa, H., Klewe-Nebenius, D., Chambers, I., Schöler, H., and Smith, A. (1998). Formation of pluripotent stem cells in the mammalian embryo depends on the POU transcription factor Oct4. *Cell* **95**, 379–391.
- Ohgushi, M., Matsumura, M., Eiraku, M., Murakami, K., Aramaki, T., Nishiyama, A., Muguruma, K., Nakano, T., Suga, H., Ueno, M., et al. (2010). Molecular pathway and cell state responsible for dissociation-induced apoptosis in human pluripotent stem cells. *Cell Stem Cell* **7**, 225–239.
- Percivalle, R.M., Stewart, D.P., Koss, B., Lynch, J., Milasta, S., Bathina, M., Temirov, J., Cleland, M.M., Pelletier, S., Schuetz, J.D., et al. (2012). Anti-apoptotic MCL-1 localizes to the mitochondrial matrix and couples mitochondrial fusion to respiration. *Nat. Cell Biol.* **14**, 575–583.
- Ploner, C., Kofler, R., and Villunger, A. (2008). Noxa: at the tip of the balance between life and death. *Oncogene* **27** (Suppl 1), S84–S92.
- Qi, L.S., Larson, M.H., Gilbert, L.A., Doudna, J.A., Weissman, J.S., Arkin, A.P., and Lim, W.A. (2013). Repurposing CRISPR as an RNA-guided platform for sequence-specific control of gene expression. *Cell* **152**, 1173–1183.
- Shalem, O., Sanjana, N.E., Hartenian, E., Shi, X., Scott, D.A., Mikkelsen, T., Heckl, D., Ebert, B.L., Root, D.E., Doench, J.G., and Zhang, F. (2014). Genome-scale CRISPR-Cas9 knockout screening in human cells. *Science* **343**, 84–87.



- Singhal, N., Graumann, J., Wu, G., Araúzo-Bravo, M.J., Han, D.W., Greber, B., Gentile, L., Mann, M., and Schöler, H.R. (2010). Chromatin-remodeling components of the baf complex facilitate reprogramming. *Cell* *141*, 943–955.
- Sokol, S.Y. (2011). Maintaining embryonic stem cell pluripotency with Wnt signaling. *Development* *138*, 4341–4350.
- Sun, Y., Paşca, S.P., Portmann, T., Goold, C., Worringer, K.A., Guan, W., Chan, K.C., Gai, H., Vogt, D., Chen, Y.J.J., et al. (2016). A deleterious Nav1.1 mutation selectively impairs telencephalic inhibitory neurons derived from Dravet Syndrome patients. *eLife* *5*, e1307.
- Takahashi, K., and Yamanaka, S. (2006). Induction of pluripotent stem cells from mouse embryonic and adult fibroblast cultures by defined factors. *Cell* *126*, 663–676.
- Takahashi, K., Tanabe, K., Ohnuki, M., Narita, M., Ichisaka, T., Tomoda, K., and Yamanaka, S. (2007). Induction of pluripotent stem cells from adult human fibroblasts by defined factors. *Cell* *131*, 861–872.
- Takashima, Y., Guo, G., Loos, R., Nichols, J., Ficiz, G., Krueger, F., Oxley, D., Santos, F., Clarke, J., Mansfield, W., et al. (2015). Erratum: resetting transcription factor control circuitry toward ground-state pluripotency in human (*Cell* (2014) 158 (1254–1269)). *Cell* *162*, 452–453.
- Vetterkind, S., and Morgan, K.G. (2009). The pro-apoptotic protein Par-4 facilitates vascular contractility by cytoskeletal targeting of ZIPK. *J. Cell. Mol. Med.* *13*, 887–895.
- Wang, W.P., Tzeng, T.Y., Wang, J.Y., Lee, D.C., Lin, Y.H., Wu, P.C., Chen, Y.P., Chiu, I.M., and Chi, Y.H. (2012). The EP300, KDM5A, KDM6A and KDM6B chromatin regulators cooperate with KLF4 in the transcriptional activation of POU5F1. *PLoS ONE* *7*, e52556.
- Wang, T., Birsoy, K., Hughes, N.W., Krupczak, K.M., Post, Y., Wei, J.J., Lander, E.S., and Sabatini, D.M. (2015). Identification and characterization of essential genes in the human genome. *Science* *350*, 1096–1101.
- Watanabe, K., Ueno, M., Kamiya, D., Nishiyama, A., Matsumura, M., Wataya, T., Takahashi, J.B., Nishikawa, S., Nishikawa, S., Muguruma, K., and Sasai, Y. (2007). A ROCK inhibitor permits survival of dissociated human embryonic stem cells. *Nat. Biotechnol.* *25*, 681–686.
- Yamanaka, S., Zhang, X.Y., Maeda, M., Miura, K., Wang, S., Farese, R.V., Jr., Iwao, H., and Innerarity, T.L. (2000). Essential role of NAT1/p97/DAP5 in embryonic differentiation and the retinoic acid pathway. *EMBO J.* *19*, 5533–5541.
- Yilmaz, A., Peretz, M., Aharoni, A., Sagi, I., and Benvenisty, N. (2018). Defining essential genes for human pluripotent stem cells by CRISPR-Cas9 screening in haploid cells. *Nat. Cell Biol.* *20*, 610–619.
- Yu, J., Vodyanik, M.A., Smuga-Otto, K., Antosiewicz-Bourget, J., Frane, J.L., Tian, S., Nie, J., Jonsdottir, G.A., Ruotti, V., Stewart, R., et al. (2007). Induced pluripotent stem cell lines derived from human somatic cells. *Science* *318*, 1917–1920.
- Zhang, Y., Schulz, V.P., Reed, B.D., Wang, Z., Pan, X., Mariani, J., Euskirchen, G., Snyder, M.P., Vaccarino, F.M., Ivanova, N., et al. (2013). Functional genomic screen of human stem cell differentiation reveals pathways involved in neurodevelopment and neurodegeneration. *Proc. Natl. Acad. Sci. U S A* *110*, 12361–12366.
- Zhao, M., Kim, P., Mitra, R., Zhao, J., and Zhao, Z. (2016). TSGene 2.0: an updated literature-based knowledgebase for tumor suppressor genes. *Nucleic Acids Res.* *44* (D1), D1023–D1031.

## STAR★METHODS

### KEY RESOURCES TABLE

REAGENT or RESOURCE	SOURCE	IDENTIFIER
<b>Antibodies</b>		
Conjugated (AF488) Rabbit anti-OCT4 (C30A3)	Cell Signaling Technologies	CST-5177; RRID:AB_10693303
Phalloidin-647	ThermoFisher Scientific	A22287; RRID:AB_2620155
Rabbit anti-scribble (SCRIB)	Abcam	ab36708; RRID:AB_777865
Rabbit anti-PKC zeta (PRKCZ)	Abcam	ab59364; RRID:AB_944858
Rabbit anti-PAR-4 (PAWR)	Cell Signaling Technologies	CST-2328; RRID:AB_561235
Rabbit anti-Cleaved Caspase-3 Asp175 (CC3)	Cell Signaling Technologies	CST-9661; RRID:AB_2341188
Mouse anti-GAPDH (ID4)	Enzo	ADI-CSA-335-E; RRID:AB_2039148
IRDye 800CW anti-rabbit	LiCOR	926-32211; RRID:AB_621843
IRDye 680RD anti-mouse	LiCOR	926-68070; RRID:AB_10956588
<b>Chemicals, Peptides, and Recombinant Proteins</b>		
thiazovivin	Selleckchem	S1459
<b>Experimental Models: Cell Lines</b>		
Human: H1-hESCs, NIHhESC-10-0043, WA01 (XY)	WiCell	H1-hESCs
Human: H9-hESCs, NIHhESC-10-0062, WA09 (XX)	WiCell	H9-hESCs
Human: 8402-iPSCs (XY)	Coriell Institute – Fibroblasts GW08402 <a href="#">Sun et al., 2016</a>	8402-iPSCs
Human: hDFN-iPSCs (XY)	ThermoFisher: Human Dermal Fibroblasts neonatal (HDFn) C0045C. <a href="#">Bidinosti et al., 2016</a>	hDFN-iPSCs
Human: transgenic H1-hESCs + dox inducible (i) Cas9	<a href="#">lhry et al, 2018</a>	H1-iCas9
Human: transgenic H1-hESCs + CAG-dCAS9-KRAB	This paper	HI-hESC CRISPRi
Human: transgenic hDFN-iPSCs + CAG-dCAS9-KRAB	This paper	HI-hDFN CRISPRi
HEK293T	ATCC	CRL-3216
<b>Oligonucleotides</b>		
Spacer Sequence for synthetic crRNA: PMAIP1 crRNA 3 TCGAGTGTGCTACTCAACTC	Alt-R® CRISPR-Cas9 crRNA, 2 nmol - IDT	N/A
Spacer Sequence for synthetic crRNA: PAWR crRNA 5 CGAGCTCAACAACAACCTCC	Alt-R® CRISPR-Cas9 crRNA, 2 nmol - IDT	N/A
Spacer Sequence for synthetic crRNA: TP53 crRNA 1 GAAGGGACAGAAGATGACAG	Alt-R® CRISPR-Cas9 crRNA, 2 nmol - IDT	N/A
Spacer Sequence for synthetic crRNA: TP53 crRNA 2 GAAGGGACAGAAGATGACAG	Alt-R® CRISPR-Cas9 crRNA, 2 nmol - IDT	N/A
Spacer Sequence for synthetic crRNA: TP53 crRNA 4 GAGCGCTGCTCAGATAGCGA	Alt-R® CRISPR-Cas9 crRNA, 2 nmol - IDT	N/A
Spacer Sequence for synthetic crRNA: P21 crRNA 1 AATGGCGGGCTGCATCCAGG	Alt-R® CRISPR-Cas9 crRNA, 2 nmol - IDT	N/A
Spacer Sequence for synthetic crRNA: P21 crRNA 4 TCCACTGGGCCGAAGAGCGG	Alt-R® CRISPR-Cas9 crRNA, 2 nmol - IDT	N/A
Spacer Sequence for synthetic crRNA: P21 crRNA 6 GGCGCCATGTCAGAACCAGC	Alt-R® CRISPR-Cas9 crRNA, 2 nmol - IDT	N/A
<b>Recombinant DNA</b>		
LentiCRISPR - Lentiviral backbone for CRISPR nuclease interference spacer sequences cloning	pNGx-LV-g003 Plasmid backbone from <a href="#">DeJesus et al., 2016</a>	pNGx-LV-g003
LentiCRISPR - Lentiviral backbone for CRISPR Genome-wide sgRNA library	pRS116 lentiviral plasmid (Collecta, Mountain View, CA) Described by <a href="#">DeJesus et al., 2016</a>	N/A
pAAVS1-CAG-dCAS9-KRAB	This paper	<a href="#">Data S1</a>

(Continued on next page)

**Continued**

REAGENT or RESOURCE	SOURCE	IDENTIFIER
Software and Algorithms		
Pooled CRISPR – Bowtie2	Langmead and Salzberg, 2012	<a href="http://bowtie-bio.sourceforge.net/bowtie2/index.shtml">http://bowtie-bio.sourceforge.net/bowtie2/index.shtml</a>
Pooled CRISPR - DESeq2 v1.10.1,	Love et al., 2014	<a href="https://bioconductor.org/packages/release/bioc/html/DESeq2.html">https://bioconductor.org/packages/release/bioc/html/DESeq2.html</a>
Pooled CRISPR - RSA release 1.8	König et al. 2007	<a href="https://admin-ext.gnf.org/publications/RSA/">https://admin-ext.gnf.org/publications/RSA/</a>
Pooled CRISPR - BAGEL	Hart and Moffat, 2016	<a href="https://sourceforge.net/projects/bagel-for-knockout-screens/">https://sourceforge.net/projects/bagel-for-knockout-screens/</a>
RNaseq - STAR aligner v2.5.1b	Dobin et al., 2013	<a href="https://github.com/alexdobin/STAR/releases/tag/2.5.1b">https://github.com/alexdobin/STAR/releases/tag/2.5.1b</a>
RNaseq - HTSeq-count v0.6.0	Anders et al., 2015	<a href="https://htseq.readthedocs.io/en/master/index.html">https://htseq.readthedocs.io/en/master/index.html</a>
RNaseq - RSEM v1.2.28	Li and Dewey, 2011	<a href="https://github.com/deweylab/RSEM/releases/tag/v1.2.28">https://github.com/deweylab/RSEM/releases/tag/v1.2.28</a>
RNaseq - DESeq2 V 1.16.1	Love et al., 2014	<a href="https://bioconductor.org/packages/release/bioc/html/DESeq2.html">https://bioconductor.org/packages/release/bioc/html/DESeq2.html</a>

**CONTACT FOR REAGENT AND RESOURCE SHARING**

Further information and requests for resources and reagents should be directed to and will be fulfilled by the Lead Contact, Robert Ihry ([robert.ihry@novartis.com](mailto:robert.ihry@novartis.com)). Certain terms in existing license agreements may restrict our ability to transfer CRISPR/Cas9-related reagents.

**EXPERIMENTAL MODEL AND SUBJECT DETAILS****Human Pluripotent Stem Cell lines**

H1-hESCs (XY) (WA01-NIHhESC-10-0043) and H9-hESCs (XX) (NIHhESC-10-0062) were obtained from WiCell. The following cell line was obtained from the NIGMS Human Genetic Cell Repository at the Coriell Institute for Medical Research: GM08402. 8402-iPSCs (XY) originated from GM08402 fibroblasts reprogrammed as described by [Sun et al. \(2016\)](#). hDFN-iPSCs (XY) were generated as described by [Bidinosti et al. \(2016\)](#). hPSC lines were free of Mycoplasma and tested using the Mycoalert Detection kit (Lonza). SNP fingerprinting confirmed the identity of hPSC lines used. Karyotyping was performed by Cell Line Genetics (Madison, WI).

**Large-scale culture of hPSCs**

H1-hESCs with AAVS1 knock in of the iCas9 transgene were generated and cultured in TeSR-E8 media (STEMCELL TECH.-05940) on vitronectin (GIBCO-A14700) coated plates as described by [Ihry et al. \(2018\)](#). Pilot studies with a sub-genome sgRNA library used a total of 40 individual T225 flasks and was cumbersome ([Ihry et al., 2018](#)). Daily feeding and passaging in which multiple flask needed to be pooled was time consuming and increased the risk for contamination. To minimize the manipulation required during feeding and passaging we used 5-layer CellSTACKs. The vessels are large enough to contain an entire 45,000 sgRNA library at > 1000x coverage per sgRNA at a seeding density of 21,000 cells/cm<sup>2</sup> (Seed 66 million cells for ~1400x). In practical terms only 4 to 8 5-layer CellSTACKs were growing at a given time during the month-long genome-scale CRISPR screen ([Figure S1](#)). Given the expense of E8 media Penicillin-Streptomycin (pen/strep) at 100 U/mL was added as an additional insurance policy for the first screen at scale. After running a lengthy genome-scale screen and becoming experienced with large-scale hPSC culture it is possible to run future screens without pen/strep.

**METHOD DETAILS****Genome Engineering**

H1-hESCs expressing dox inducible (i) iCas9 were generated by [Ihry et al. \(2018\)](#). Dox treated H1-iCas9 cells were subjected to three successive rounds of RNAi delivery of the two-component synthetic crRNA/tracrRNA (IDT) pairs targeting *PMAIP1*, *PAWR*, *P21* (*CDKN1A*) and *TP53* as described by [Ihry et al. \(2018\)](#). *PMAIP1*, and *PAWR* were transfected with a single sgRNA while *TP53* and *P21* were co-transfected with 3 crRNAs. CRISPR indel analysis detected efficient gene disruption for all three genes and was performed as described by [Ihry et al. \(2018\)](#).

PMAIP1 crRNA 3 TCGAGTGTGCTACTCAACTC  
 PAWR crRNA 5 CGAGCTCAACAACAACCTCC  
 TP53 crRNA 1 GAAGGGACAGAAGATGACAG  
 TP53 crRNA 2 GAAGGGACAGAAGATGACAG  
 TP53 crRNA 4 GAGCGCTGCTCAGATAGCGA  
 P21 crRNA 1 AATGGCGGGCTGCATCCAGG  
 P21 crRNA 4 TCCACTGGGCCGAAGAGGCGG  
 P21 crRNA 6 GGCGCCATGTCAGAACC GGC

### **lentiCRISPR packaging**

For a one-layer CellSTACK 42 million HEK293T (66,000 cells/cm<sup>2</sup>) were plated in 100 mL of media (DMEM +10% FBS + 1x NEAA, no pen/strep). One day after seeding, cells were transfected with single lentiCRISPR plasmids in 6-well plates or pooled lentiCRISPR plasmids in CellSTACKs. For a one-layer CellSTACK 102  $\mu$ L of room temp TransIT (Mirus MIR 2700) and 3680  $\mu$ L Opti-MEM (Invitrogen 11058021) were mixed incubated in a glass bottle for 5 minutes at room temp. 94.5  $\mu$ g of Lentiviral Packaging Plasmid Mix (Cellecra CPCP-K2A) and 75.6  $\mu$ g of the lentiCRISPR plasmid library was added to the transfection mix and incubated for 15 minutes at room temp. After incubation, the mix was added to 100 mL of fresh media and the cells were fed. The next day the transfected cells received 100 mL fresh media. After 3 days of viral production supernatants were filtered (.45 $\mu$ M corning 430516) and aliquoted in to 1ml tubes for storage at  $-80^{\circ}$  C.

### **Large-scale transduction of hPSCs**

We conducted a genome-scale CRISPR screen using a 91,726 sgRNA library ( $\sim$ 5 sgRNAs per gene, split into two sgRNA sub-pools (DeJesus et al., 2016). We desired > 1000x coverage of each sgRNA to offset cell loss from double strand break (DSB)-induced toxicity (Ihry et al., 2018). To screen a sufficient number of cells we infected hPSCs with lentiCRISPRs in 5-layer CellSTACKs. Cells were infected at 0.5 MOI to ensure each cell was infected with no more than a single sgRNA. After puromycin selection cells were expanded for one week without dox to be pelleted for DNA, banked or screened (Figures 1A and S1).

Pooled CRISPR screens rely on cells being efficiently transduced at less than or equal to 0.5 MOI. We developed a reverse transfection method for hPSCs without polybrene that resulted in an efficient transduction with low volume exposure to HEK293T lentiviral supernatants. LentiCRISPR plasmids expressed a constitutive RFP and puromycin resistance to mark and select for infected cells respectively. Viral titer of the two  $\sim$ 45,000 sgRNA libraries expressing RFP in 6-well plates determined that less than 25  $\mu$ L in 1.5mL of media was required for 0.5 MOI. These calculations scaled appropriately in 5-layer cell stacks with 500 mL of media and approximately 50% of the cells were RFP positive in the absence of puromycin.

A genome-scale lentiCRISPR library targeting each gene 5 times has been split into  $\sim$ 45,000 sub-pools (pool 1 and 2). To screen at > 1000x per sgRNA, 264 million hPSCs are infected in 4x 5-layer CellSTACKS (12,720 cm<sup>2</sup>, 21,000 cells/cm<sup>2</sup>). 2 stacks equal one replicate. Cells are infected at 0.5 MOI to ensure only one sgRNA is expressed per cell (+sgRNA/puro<sup>R</sup>/RFP). After puromycin selection cells are expanded until confluent (4-6 days). At this point 40 million cells (10 million/ml) can be banked in 5ml cryovials for use at a later date.

### **Banking lentiCRISPR infected hPSC library**

One 5-layer cell stack was treated with 200 mL accutase that was evenly distributed among layers. After incubation at 37 C for 10 minutes, accutase (GIBCO-A1 110501) was neutralized with 200 mL E8 media. Cells were counted and pelleted to be resuspended at a concentration of 10 million cells per ml in a solution of 40% Tet-free FBS (Seradigm #1500-500) and 10% DMSO (Sigma D2650) and 50% E8 media. 4 mL aliquots were placed in 5 mL cryovials and frozen in a Mr. Frosty (Thermo Scientific 5100-0050) at  $-80^{\circ}$  C overnight before long-term storage in liquid nitrogen. Thawing of cells banked in 5ml cryovials showed an average viability around 85% for both lentiCRISPR pools. Viability was assayed using a Nexcelom Cellometer Auto 2000 and AO/PI (Nexcelom CS2-0106) staining solution.

We tested the effect of freezing and thawing on the representation of the sgRNAs in the library by thawing the cell library at 2700x (120 million cells per 45k sub-pool) cells per sgRNA. Cells were thawed in a 37 C water bath and transferred to a 50 mL conical with E8 media and centrifuged at 300 g for 3 minutes. Pelleted cells were resuspended in E8 media and replated at a density of 40,000 to 60,000 cells/cm<sup>2</sup>. 3 cryovials with 120 million cells was thawed and plated on a 5-layer cell stack (120,000,000 /45,000 = 2700x).

After thawing and feeding the cells for two days, DNA was isolated and analyzed by NGS to measure the representation of each sgRNA in the pool. Both day zero and freeze/thaw samples had an over 87% alignment of sequencing reads and fewer than 25 missing barcodes per replicate. Pearson correlation analysis allowed us to demonstrate that there was a high correlation between the day zero samples and the freeze/thaw samples. Calculating normalized sgRNA counts revealed a strong correlation between the cell library before (day 0) or after one freeze/thaw cycle (Figure 1B).

### **Pooled Mutagenesis (CRISPR nuclease/interference)**

H1-hESCs expressing a constitutive (c) Cas9-KRAB knocked-in to the AAVS1 locus were generated as described by Ihry et al. (2018). The following lentiCRISPR were used to transduce iCas9 or cCas9-KRAB cells to generate mutant cell pools.



### CRISPR nuclease

PAWR sgRNA 1 TTTGGGAATATGGCGACCGG  
 PAWR sgRNA 2 GGTGGCTACCGGACCAGCAG  
 PAWR sgRNA 5 CGAGCTCAACAACAACCTCC  
 MAPT sgRNA 1 GAAGTGATGGAAGATCACGC  
 ACSL4 sgRNA TGGTAGTGGACTCACTGCAC  
 ARSH sgRNA GCAGCACCGTGGCTACCGCA  
 BMX sgRNA ATGAAGAGAGCCGAAGTCAG  
 BTK sgRNA GGAATCTGTCTTTCTGGAGG  
 GABRA3 sgRNA AAGGACTGACCTCCAAGCCC  
 GK sgRNA TAGAAAGCTGGGGCCTTGGA  
 NRK sgRNA CGCCTTCCTATTTTCAGGTAA  
 TLR7 sgRNA CAGTCTGTGAAAGGACGCTG

### CRISPR interference

Control-2 GACCGGAACGATCTCGCGTA  
 PAWR sgRNA 1 GGCGCGCTCGAGGACTCCAA  
 PAWR sgRNA 2 GTTGCAGGGTGGGGACCCGG  
 PAWR sgRNA 3 GCTGGCCGGTAGTACTGGT  
 PAWR sgRNA 5 GGCTGCTGGCCGGTAGTGAC

### OCT4 FACS-BASED screen

Cells were dissociated using accutase for 10 min at 37 C to create a single-cell suspension which was strained using a 40-micron filter and was counted. After removing accutase, pelleted cells were resuspended in a volume of 1 million cells/mL for the staining protocol. For each replicate 55 million unsorted cells were frozen down prior to fixation. The remaining cells were fixed in 4% PFA in PBS for 10 minutes at room temperature on a rocker. Cells were spun down at 300 RCF for 3 min between each subsequent solution change. Cells were washed with 0.1% Triton-X in PBS after fixation and blocked in 2% goat serum, 0.01% BSA and 0.1% triton X in PBS for 1hr at room temperature. Conjugated (AF488) primary antibodies specific to OCT4 (CST 5177) were diluted in blocking solution (1:200) and incubated with cells on a rocker over night at 4 C. Prior to FACS analysis cells were resuspended in PBS at a concentration of 30 million cells/mL. A total of 1.2 billion cells (both replicates) were sorted into OCT4<sup>low</sup> (50 million cells) and OCT4<sup>high</sup> (61 million cells) populations using an ARIA III (BD).

### DNA isolation and NGS libraries

For each replicate, 55 million cells (~1200x) were pelleted and genomic DNA was isolated using QIAamp DNA Blood Maxi Kit (QIAGEN 51194) as directed by manufacturer. Isolating genomic DNA from 4% PFA fixed cells was performed by utilizing phenol chloroform extraction. Cells were resuspended in 500ul TNES (10mM Tris-Cl ph 8.0, 100mM NaCl, 1mM EDTA, 1% SDS) and incubated overnight at 65 C. After allowing the samples to cool, 10ul of RNase A (QIAGEN 19101) and samples were incubated at 37 C for 30 minutes. Next, 10ul of proteinase K (QIAGEN 19133) and incubated for 1 hour at 45 C. Add 500ul of PCIA (Phenol;Cholorform; Isoamyl alcohol ph 8) (Thermo 17908) and vortex. Spin samples in a centrifuge at max speed for 2 minutes. Transfer the aqueous phase to 500ul of PCIA and vortex. Spin at max speed for 2 minutes. Transfer the aqueous phase to 450ul of chloroform and vortex. Spin at max speed for 2 minutes. Transfer aqueous phase to 40ul of 3M NaAcO ph 5.2. Add 1 mL of 100% ethanol, mix and precipitate DNA for 1 hour on ice. Spin at max speed for 2 minutes. Decant and wash with 1ml 70% ethanol. Spin at max speed for 1 minutes. Decant and air dry the pellet. Resuspend in 50ul of nuclease free H<sub>2</sub>O. PCR was performed using lentiCRISPR specific primers and library construction and sequencing was performed as described by [DeJesus et al. \(2016\)](#).

### mRNA expression

qPCR and RNA-seq analysis were performed as described by [Ihry et al. \(2018\)](#). Median TPM values for H1-hESCs are available upon request. RNA-seq data for in 4 iPSC control lines subjected to NGN2 differentiation is available upon request but is restricted to the expression for *PAWR* and *PMAIP1*.

### Assaying sensitivity to DNA damage

Control and mutant iCas9 H1-hESCs expressing a *MAPT* targeting sgRNA were monitored daily post-media change using an IncuCyte zoom (Essen Biosciences). At the onset of the experiment cells were plated at density of 10,500 to 21,000 cells/cm<sup>2</sup> and cultured plus or minus dox for the duration. Confluence was calculated using the processing analysis tool (IncuCyte Zoom Software).

### Assaying survival without ROCK inhibitor

Control and mutant iCas9 H1-hESCs were dissociated with accutase for 10 minutes. Flowmi 40-micron cell strainers (BEL-ART H13680-0040) were used to ensure a uniform single-cell suspension prior to replating cells. Cells were plated at a density of 10,500 to 21,000 cells/cm<sup>2</sup> plus or minus thiazovivin (ROCK inhibitor, Selleckchem, S1459). Timelapse images were taken in 3 hr intervals using IncuCyte zoom (Essen Biosciences). The confluence processing analysis tool (IncuCyte Zoom Software) calculated confluency for each sample.

### Immunofluorescence and Western Blotting

Immunofluorescence staining of fixed cells was performed as described by [Ihry et al. \(2018\)](#). Protein lysates were made by vortexing cell pellets in RIPA buffer (Thermo Scientific 89901) supplemented with Halt protease inhibitor cocktail (Thermo Scientific 78430) and phosphatase inhibitors (Thermo Scientific 1862495). Samples were incubated at 4C for 10 minutes before centrifugation at 14,000 x g for 10 minutes at 4C. Supernatants were transferred to new tubes and quantified using the BCA protein assay kit (Thermo Scientific 23225) and a SpectraMax Paradigm (Molecular Devices) plate reader. Samples were prepared with NuPAGE LDS sample buffer 4x (Invitrogen NP0008) and NuPAGE sample reducing agent (Invitrogen NP0009) and heated for 10 minutes at 70 C. Chameleon Duo Pre-stained Protein Ladder (LiCOR P/N 928-60000) was loaded alongside 10 ug of protein per sample on a NuPAGE 4%–12% Bis-Tris Protein Gels, 1.5 mm, 10-well (Invitrogen NP0335BOX). Gel electrophoresis was performed at 150 V for 1hr in NuPAGE MOPS SDS Running buffer (20X) (Invitrogen NP0001) using a XCell SureLock Mini-Cell (Thermo Scientific EI0002). Transfer was performed using an iBlot 2 dry blotting system (Thermo IB21002 and IB23002) as described by manufacturer. Blots were blocked in TBS blocking buffer (LiCOR 927-50000) for 1 hour at room temperature. The blots were then incubated with primary antibodies diluted in TBS over night at 4 C. Blots were washed 3X in PBST and incubated with secondary antibodies diluted in TBS for 2 hours at room temperature. Blots were imaged using an Odyssey CLx (LiCOR).

### Primary antibodies

Phalloidin-647 (ThermoFisher Scientific A22287) - 1:40  
SCRIB (Abcam ab36708) - 1:100 (IF)  
PRKCZ (Abcam ab59364) - 1:100 (IF)  
PAWR/PAR-4 (CST-2328) - 1:100 (IF)  
Cleaved Caspase-3 Asp175 (CST-9661) - 1:200 (IF) 1:1000 (WB)  
GAPDH (Enzo ADI-CSA-335-E) - 1:1000 (WB)

### Secondary Antibodies

IRDye 800CW anti-rabbit (LiCOR 926-32211) - 1:5000  
IRDye 680RD anti-mouse (LiCOR 926-68070) - 1:5000  
AF488 conjugate Goat anti-Rabbit IgG (H+L) (ThermoFisher-A-11008) - 1:500

## QUANTIFICATION AND STATISTIC ANALYSIS

### Figures 1B and 7A

The scatterplot in 1B depicts the average normalized count values ( $n = 2$  replicates) for sgRNA barcodes ( $\sim 91,000$  sgRNAs) in two conditions marked by the X- and y axis. The heatmap in 7A depicts Pearson correlation coefficients calculated using average normalized sgRNA counts from [Hart et al. \(2015\)](#) and this study. 1B: The r-square values were calculated as the square of standard correlation in R 7A: The r-square values were calculated as the square of standard correlation in R.

### Figures 1D, 2A, and 6B

Redundant siRNA activity (RSA) analysis is a statistical method used to calculate a p values based on the activity ranked distribution of all sgRNAs targeting a single gene ([König et al., 2007](#)) (<https://admin-ext.gnf.org/publications/RSA/>, [https://admin-ext.gnf.org/publications/RSA/RSA\\_tutorial.pdf](https://admin-ext.gnf.org/publications/RSA/RSA_tutorial.pdf)). This probability-based method favors genes with multiple active sgRNAs over a single but very active sgRNA. RSA scores each gene by identifying a bias in the distribution of sgRNAs targeting that gene. Two replicates per condition were sequenced and the raw sgRNAs counts for the genome-wide library ( $\sim 91,000$  sgRNAs) were used to calculate  $\log_2(\text{fold change})$  by DESeq2 ([Love, Huber and Anders, 2014](#)).  $\log_2(\text{fold changes})$  for the entire sgRNA library were used as the ranked distribution for RSA analysis. In this study two independent replicates with high coverage ( $\sim 1000$  cells per sgRNA) were chosen because hPSC media is prohibitively expensive at genome-scale for the month-long screen.

### Figure 1E

The BAGEL statistical model was used to calculate Bayes Factor scores and Precision Recall analysis (<http://bagel-for-knockout-screens.sourceforge.net/>).  $\log_2(\text{Fold Change})$  of raw sgRNA counts were used as input to for BAGEL analysis.

**Figures 3B and 3E**

Statistical analysis of relative expression values generated by qPCR for *PMAIP1* (3B) *P21* (3E) and *FAS* (3E) mRNAs was conducted using PRISM software (version 7.0c). Relative expression values for control and treated samples were tested for statistical differences by conducting an ordinary unpaired two tailed t test with equal variance.  $n = 3$  for control and treated mRNA samples isolated from 3 independent wells are plotted as individual dots. Bars indicate mean and error bars depict standard deviation. \* $p < 0.05$ , \*\* $p < 0.01$ , \*\*\* $p < 0.001$ , \*\*\*\* $p < 0.0001$ .

**Figure 3A and S4F**

Differential gene expression was performed in R with DESeq2 which is suitable for studies with three replicates ( $n = 3$ ), and maintains high precision and sensitivity (Love, Huber and Anders, 2014). Gene counts are normalized for library size using the geometric mean and modeled with a negative binomial distribution. RNA was isolated from 1-4 independent samples for both control and Ngn2 neuronal samples in different hPSC backgrounds (H1-hESCs ( $n = 1$ ), H9-hESCs ( $n = 3$ ), 8402-iPSCs ( $n = 3$ ) and HDFn-iPSCs ( $n = 4$ )).

**DATA AND SOFTWARE AVAILABILITY**

RNaseq data in hPSCs and Ngn2 neurons is limited to the expression of *PMAIP1* and *PAWR* and is available upon request. Normalized sgRNA counts, Log<sub>2</sub>(fold changes) and RSA analysis for pooled CRISPR screens in H1-hESCs are available in Tables S1, S2, S3, S5 and S8. Pooled CRISPR screening data in cancer cell lines is limited to Log<sub>2</sub>(fold changes) for *PMAIP1* sgRNAs and is available upon request. RNA-seq data processing and pooled CRISPR NGS were conducted using open source software as indicated in the key resources table.